DETECTION OF NEAR-SURFACE ANISOTROPY IN A WEATHERED METAMORPHIC SCHIST USING TIME-DOMAIN ELECTROMAGNETICS

A Thesis

by

JAMIE LYNNE COLLINS

Submitted to the Office of Graduate Studies of
Texas A&M University
in partial fulfillment of the requirements for the degree of

MASTER OF SCIENCE

August 2004

Major Subject: Geophysics

DETECTION OF NEAR-SURFACE ANISOTROPY IN A WEATHERED METAMORPHIC SCHIST USING TIME-DOMAIN ELECTROMAGNETICS

A Thesis

by

JAMIE LYNNE COLLINS

Submitted to Texas A&M University
in partial fulfillment of the requirements
for the degree of

MASTER OF SCIENCE

Approved as to style and content by:

Mark E. Everett (Chair of Committee)	Brann Johnson (Member)
Cristine Morgan (Member)	Richard Carlson (Head of Department)

August 2004

Major Subject: Geophysics

ABSTRACT

Detection of Near-Surface Anisotropy in a Weathered

Metamorphic Schist Using Time-Domain Electromagnetics. (August 2004)

Jamie Lynne Collins, B.S., Texas A&M University

Chair of Advisory Committee: Dr. Mark Everett

Controlled-source, azimuthal, time-domain, electromagnetic (TDEM) surveys were conducted over a schist formation with uniformly striking, nearly vertical foliation. Direct current electrical resistivity and seismic refraction surveys provided additional independent assessment of the field site. Quantitative interpretation of the TDEM survey used a theoretical electromagnetic model of a vertical transverse anisotropic conducting half-space. The combination of forward modeling and azimuthal acquisition geometry provides an innovative geophysical technique useful for mapping poorly exposed metamorphic terrains, and possibly determining fracture system orientations and assessing anisotropic hydraulic conductivity.

Metamorphic rocks may exhibit transverse electrical anisotropy detectable by time-domain electromagnetics due to the characteristics of foliated rocks. For this reason, the field site was chosen within the Packsaddle Schist exposed in Mason County, Texas. Foliation of the Packsaddle Schist at the survey site strikes 146º and dips 82º NE. Polar plots of early-time, TDEM voltages, measured at large transmitter-receiver separations (> 40m) exhibit a symmetric two-lobed curve that agrees with theoretical model responses calculated for a vertical transverse anisotropic half space. The long axis of the symmetric two lobe response function is oriented 137º, which is nearly parallel to schist foliation of 146º. A best-fit forward model to the data indicates the electrical conductivity parallel

and perpendicular to foliation are 0.015 S/m and 0.0012 S/m, respectively. Small transmitter-receiver separations (< 40m) exhibit azimuthal responses typical of an isotropic half space, which indicates the presence of a layer overlying the schist probably produced by weathering.

An additional independent azimuthal Wenner resistivity survey exhibits apparent resistivity in the form of an ellipse with the major axis (direction of maximum conductivity) oriented 149º, which is nearly parallel to schist foliation of 146º. Analysis of data indicates the apparent electrical conductivity parallel and perpendicular to foliation are 0.0163 S/m and 0.0094 S/m, respectively. Results of TDEM and direct current resistivity closely match in both orientation and electrical conductivity values. Preliminary seismic refraction data were compatible with the TDEM data and also indicated anisotropy, but were not as conclusive.

ACKNOWLEDGMENTS

I would like to thank my advisor Mark Everett for keeping me calm and patiently answering each and every one of my questions no matter how obvious they may have been.

I would also like to thank Brann Johnson for encouraging me to think outside the box and providing the research location, geologic knowledge of the area, and help during the writing process.

For the generous use of their land, I would like to thank Gary and Carole Zesch and Mike and Diana Dial.

For braving the cactus and helping me complete my surveys, I would like to thank Austen Crider, Neelambari Save, Josh King, Luke Cooper, Clark Ferley, and Jennifer Collins.

Carl Pierce, and Alfonso Benevidas deserve recognition for their patience in answering my numerous equipment and technical problems.

Finally, I would like to recognize my parents for their emotional and financial support throughout the whole process.

TABLE OF CONTENTS

Page

LIST OF FIGURES

FIGURE Page

LIST OF TABLES

INTRODUCTION

Time-domain electromagnetics (TDEM) is thought to provide a useful, noninvasive geophysical technique to map anisotropy in buried crystalline rocks. Such a technique could serve to indicate the strike of foliation in metamorphic terrains, or provide information about geologic structures, stress history, fluid flow, degree of weathering, and many other geologic factors. These factors are detectable with azimuthal TDEM data if they exhibit sufficient electrical anisotropy. Previous studies of electrical anisotropy have used direct current, azimuthal resistivity methods [*Busby*, 2000; *Watson and Barker*, 1999]. In addition, theoretical studies have modeled the electromagnetic response of different anisotropic media [*Yu and Edwards*, 1992; *LeMasne and Vasseur*, 1981]. Combining numerical modeling with azimuthal TDEM acquisition in this study could lead to confident geological interpretation of the mechanisms generating electrical anisotropy in buried crystalline rocks.

Investigating anisotropic TDEM responses requires geology that can be represented by an anisotropic model of electrical conductivity. A simple model assumes homogeneity and vertical transverse anisotropy in which two principal components of electrical conductivity, σ_{11} and σ_{22}, lie in the same vertical plane, are perpendicular, and equal ($\sigma_{\|}$). A third principal component of electrical conductivity, σ_{33}, is perpendicular and not equal to σ_{11} and σ_{22} ($\sigma_{\perp}$). In an idealized situation, a steeply dipping foliated

---

This thesis follows the style and format of *Journal of Geophysical Research*.

metamorphic rock formation could possess parameters of a simple model and provide ideal conditions for a field-scale experiment. Our study site has been selected within the foliated Packsaddle Schist of the Llano uplift in central Texas. The geology at the site is simple and assumed to have the appropriate attributes to potentially exhibit nearly vertical transverse anisotropy and spatial homogeneity.

Multiple TDEM azimuthal surveys using different transmitter-receiver (TX-RX) separations were conducted at the study site to determine if the anticipated vertical transverse anisotropy is exhibited. Varying the measurements by azimuth constrains the symmetry of anisotropy, and different TX-RX separations explore various depths of investigation. In addition to TDEM surveys, direct current resistivity and seismic surveys were conducted to in order to provide additional independent assessment of anisotropic behavior, and help discriminate between different sources of anisotropy. The numerical modeling aspect of our study is based on the theory in *al-Garni and Everett* [2003], re-casting the frequency domain electromagnetic response into the time domain.

The TDEM data vary with azimuth, showing the dependence of RX voltage on TX-RX orientation with respect to across-strike conductivity, $\sigma_{\perp}$, and along-strike conductivity, $\sigma_{||}$. Polar plots of the early-time voltage response exhibit a two-lobed shape, with the maximum principal axis of the lobes oriented northwest-southeast. Early-time voltage is high in resistors indicating the maximum principal axis is the most resistive direction; however, the paradox of anisotropy indicates the reverse is true [*al-Garni and Everett*, 2003]. In actuality, higher conductivity is in the direction of the maximum principal axis, which is approximately the same direction as the measured

foliation of the Packsaddle Schist. The shape of the response is in good agreement with the prediction of numerical models.

Causes of the electrical anisotropy detected by TDEM are investigated and narrowed with the application of previous seismic anisotropy studies. Properties of foliated rocks such as mineral foliation, mineral lamination, compositional banding, grain boundary cracks, or a combination of these are believed to cause both elastic and electrical vertical transverse anisotropy at the field site. In addition, Recent/Holocene and Cambrian-age weathering along with systematic fracture systems have affected the field site and, hence, the vertical transverse anisotropic behavior of a schistose rock mass. Considering the possible causes of anisotropy, the combination of azimuthal TDEM acquisition and modified modeling in this study suggests a useful noninvasive technique to detect vertical transverse anisotropy.

PREVIOUS STUDIES

Direct current (DC) geoelectric soundings have been used for over 50 years to measure electrical resistivity, or inversely the electrical conductivity, of the subsurface. *Bhattacharya and Patra* [1968] recognized the effect of anisotropy on the flow of electric currents in the subsurface. Mineral crystal shape, sedimentary structures, and weathering were cited as possible causes of anisotropy. To represent vertical transverse anisotropy in two dimensions, two principal components of a second rank tensor of resistivity were used. Longitudinal resistivity ρ_s is the resistivity parallel to the plane of stratification, and transverse resistivity ρ_t is that perpendicular to the plane of stratification. Computations with these two parameters led *Bhattacharya and Patra* [1968] to identify a "paradox of anisotropy" in direct current resistivity. The paradox arises when apparent resistivity normal to the strike direction is less than along the strike direction, which is opposite to actual resistivity due to the accumulation of charges in the across-strike direction. Recently, *Watson and Barker* [1999] differentiated anisotropy and spatial variations using azimuthal, resistivity offset, Wenner soundings. Their research addressed concerns with the assumptions made in previous studies that azimuthal variations in apparent resistivity signify anisotropy, without consideration of spatial variability. To show the influence of spatial heterogeneity, *Watson and Barker* [1999] demonstrated that DC resistivity azimuthal data are affected by systematic fracture systems along with dipping stratigraphy and lateral formation changes.

Electromagnetics also measures electrical conductivity, but offers many advantages over direct current resistivity surveying. These advantages have lead to an

increased implementation of electromagnetic induction (EM). *Le Masne and Vasseur* [1981] showed theoretically and experimentally that transverse anisotropy can be measured using frequency-domain electromagnetics (FDEM). A fissured limestone with vertical, parallel fractures was used to demonstrate subsurface anisotropy. Their study was able to define the direction and magnitude of conductivity more rapidly and accurately than the direct current method. *Yu and Edwards* [1992] studied the theoretical controlled-source electromagnetic effects of transverse anisotropy on the oceanic lithosphere. TDEM responses of a two layer model were theoretically computed where an upper half-space is sea water and a lower half-space represented an anisotropic crust of fissured basalt near an oceanic ridge. Results showed two distinct changes in the transmitter response over time. The first change was associated with the diffusion of the TDEM field through the anisotropic sea floor, and the second was because of diffusion through conductive seawater [*Yu and Edwards,* 1992]. Based on computations alone, *Yu and Edwards* [1992] concluded that anisotropy can be determined when measuring the initial TDEM response as a function of azimuth. *Al-Garni and Everett* [2003] studied a set of vertical fractures using FDEM (Figure 1). This study calculated the response of a Geonics EM34 type instrument. Results (Figure 2) revealed an apparent conductivity dependent on the angle of orientation between the transmitter and receiver loops with respect to the fracture anisotropy. The “paradox of electrical anisotropy” is evident by the higher apparent conductivity across the strike of anisotropy and a lower apparent conductivity along the strike of anisotropy, which is opposite of what actually exists [*al-Garni and Everett*, 2003].

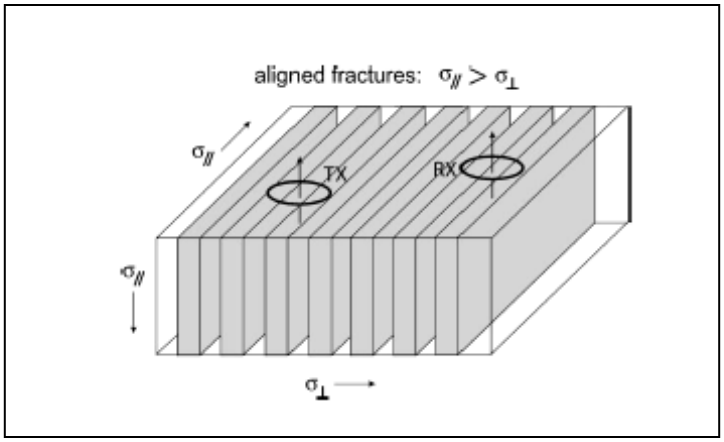

Figure 1. Model of vertical fractures causing anisotropy. A frequency-domain TX-RX loop-loop prospecting system was deployed over this half space to model the response. Along-strike conductivity $\sigma_{\|}$ is greater than across-strike conductivity $\sigma_{\perp}$ [*al-Garni and Everett*, 2003].

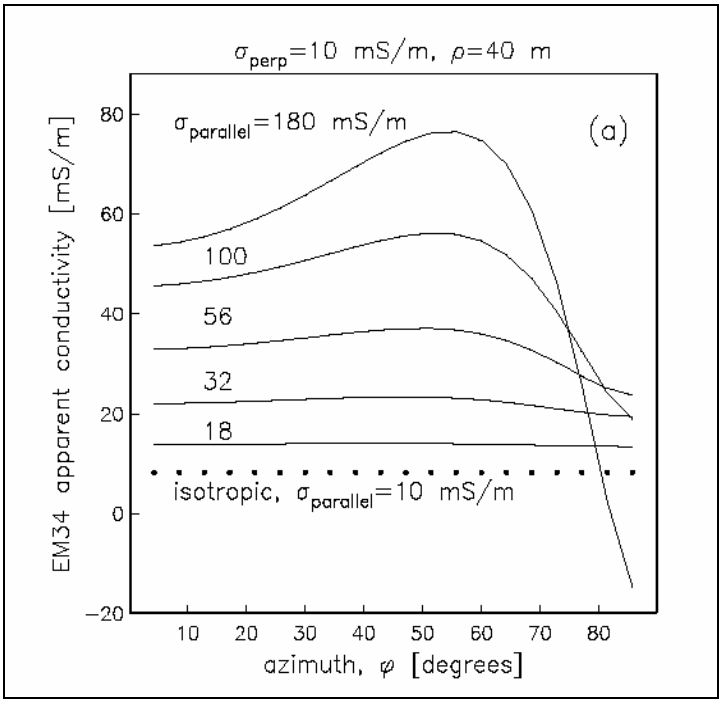

Figure 2. Theoretical FDEM apparent conductivity as a function of azimuth. Calculations numerically modeled the FDEM response over a half-space idealized as a set of vertical fractures (Figure 1). Along-strike azimuth corresponds to $\varphi = 90^{o}$ and across-strike azimuth corresponds to $\varphi = 0^{o}$ [*al-Garni and Everett*, 2003].

Previous studies of electrical anisotropy reveal the dependence of electrical conductivity on azimuth relative to the direction of anisotropy. In addition, a paradox of anisotropy has been seen to play a role in the interpretation of both resistivity and EM measurements. Computational theory determining the effect of an anisotropic half-space has been researched in direct current resistivity, frequency-domain EM, and time-domain EM methods. However, metamorphic schist has not yet been modeled as an anisotropic half-space. In addition, field measurements over an anisotropic half-space have not been collected using TDEM. Therefore, this study will determine if detection of electrical anisotropy in metamorphic schists is possible with TDEM and compare the results with predicted time-domain, numerical modeling based on the theory presented in the paper by *al-Garni and Everett* [2003].

FIELD SITE DESCRIPTION

Location and Geology of Site

The study site is located on the northwest flank of the Llano uplift, which is an exposure of ~9,000 km^2 of Precambrian igneous and metamorphic rocks in central Texas (Figure 3) [*Moser*, 1993]. The Packsaddle Schist is the youngest of the Precambrian regional metamorphic rocks. It is a metasedimentary unit estimated to be about 7,000 feet thick with spatial variability in composition and texture [*Mutis-Duplat,* 1982]. Uranium-Lead Zircon dates indicate the Packsaddle Schist is approximately 1.2 billion years old [*Moser,* 1993].

The study site is located approximately 3 km northwest of Mason, Texas (Figure 4). The bedrock at the site is the foliated Packsaddle Schist (Figure 5). Outcrops at the field site indicate that foliation of the schist is uniformly oriented with a measured strike of 146º and dip of 82º NE (Figure 6). It is hypothesized that the uniform strike and very steep dip can be represented by a vertically transverse anisotropic half-space. At the study site, the Packsaddle Schist displays foliation produced by the parallel orientation of minerals and banding or gneissic texture due to the segregation of minerals in thin layers (Figure 7). Alternating bands of light and dark minerals indicate a felsic composition of quartz and feldspar along with a mafic composition of biotite and hornblende. Discontinuous, short, white quartz veins cut the schist but form only a minor rock component at the field site. Located 100 m to the south of the study site is the unconformity between the Packsaddle Schist and the overlying Hickory Sandstone member of the Upper Cambrian Riley Formation (Figure 4). Extensive Cambrian-age, paleo-weathering of the Packsaddle Schist at the study site is exemplified by the

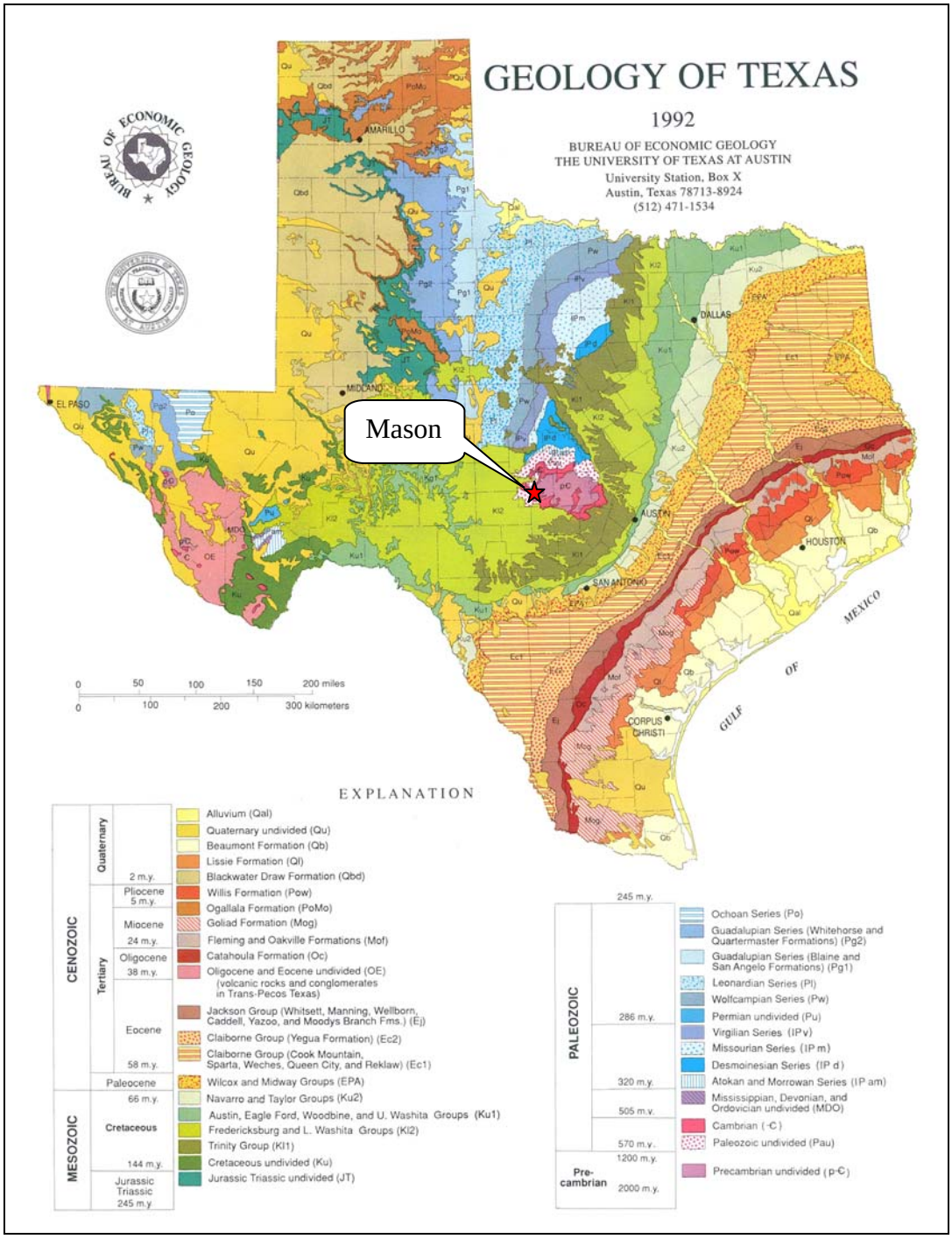

Figure 3. Geologic map of Texas. The red star indicates the approximate location of the city of Mason which is located 3 km southwest of the field site. The Llano uplift shows the exposure of Precambrian (pink) and Cambrian (red) rock units.

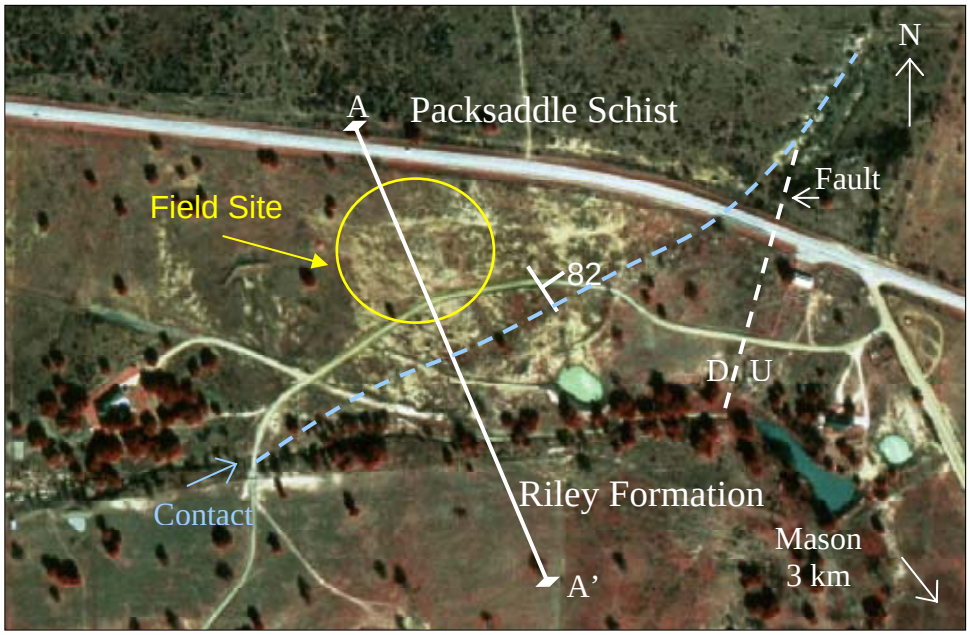

Figure 4. Aerial photograph of field site in Mason County, Texas. Basic geologic interpretation shows the known subsurface location of the Packsaddle Schist, strike and dip of foliation, the location of the Riley formation contact, and a major fault on the East. [*www.tnris.us.st.tx.com*, 2004]

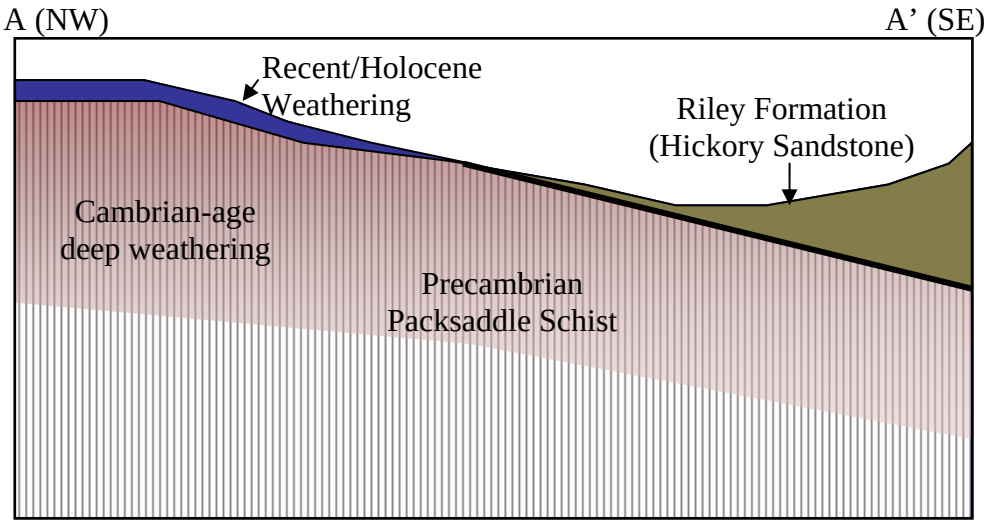

Figure 5. Vertical cross section of field site. A schematic cross section illustrating the subsurface at the field site from A to A' (Figure 4). Towards the northwest, the Packsaddle schist is overlain by a weathered layer produced in the Recent/Holocene. The Riley Formation basal contact is located to the southeast. Cambrian-age weathering of the Packsaddle Schist extends deep and decreases with depth, but the thickness and vertical variations are uncertain.

Figure 6. Outcrop of weathered Packsaddle Schist. Measured foliation trends 146º. (a) Compositional layering of mafic and felsic minerals is evident from the light and dark bands in the top picture. (b) The maroon color indicative of Cambrian-age paleoweathering is seen in the bottom picture.

Figure 7. Samples of Packsaddle Schist. (a)The top picture shows compositional banding in an oblique view and the results of Recent/Holocene weathering and Cambrian-age weathering. This sample was collected at the outcrop shown in Figure 6a. (b) The bottom picture shows the alignment of platy minerals producing foliation. The differences in these samples help demonstrate the spatial variability of the Packsaddle Schist.

character of the weathering. The mafic minerals have oxidized to a deep maroon color, not characteristic of weathering today. The weathering is interpreted to be a Cambrian-age weathering zone preserved beneath the Riley Formation. The paleo-weathering effects are believed to extend deeper than present weathering, and have been observed at other locations [*Mutis-Duplat*, 1982; *Brann Johnson personal communication, Department of Geology and Geophysics, Texas A&M University*, 2004]. In addition to weathering, multiple fracture sets not parallel to foliation have been observed but their spatial distribution is unknown.

It is important to note that the faults and systematic fracture sets along with Cambrian-age weathering of the Packsaddle Schist can affect the bulk anisotropy at the field site. Understanding the geologic history of the Packsaddle Schist provides an insight into how these and other properties can affect the electrical conductivity of the area.

Measuring Electrical Responses of an Anisotropic Medium

Detection of anisotropy using transient electromagnetics requires the subsurface to exhibit anisotropic characteristics of electrical conductivity. Several geologic properties can affect the electrical characteristics within a half-space, and therefore the anisotropy. Examples include bedding planes, systematic fractures or joints, and foliation. Our interest in this study is the cause of vertically transverse anisotropy. Possible factors contributing to the electrical anisotropy of the foliated Packsaddle Schist at the survey site include (a) mineral foliation; (b) compositional banding; (c) grain boundary cracks; (d) weathering (may increase size and number of grain boundary

cracks); and (e) systematic fracture systems (Figure 8). Relict bedding planes from the Packsaddle sediments could possibly produce anisotropy. However, bedding planes produce an anisotropy that varies vertically, unlike the lateral variations of anisotropy due to foliations. Detecting vertical variations will not be included in the scope of this study. The above factors may add or subtract from the bulk electrical anisotropy at the survey site. The specific contributions will be considered separately and tested using TDEM, direct current resistivity, and seismic methods.

At the study site, the Packsaddle Schist exhibits well-defined, mineral foliation that trends 146º and has an 82º NE dip. Composition of the schist includes quartz, feldspars, micas, and hornblende. Parallel arrangements of the minerals constitute the foliation. Previous studies have also found these minerals to be anisotropic to ultrasonic waves at the crystal scale [*Godfrey et al.*, 2000]. Therefore, the alignment of the anisotropic minerals during development of the foliation results in an anisotropic behavior of the aggregate. If elastic anisotropy is assumed to be caused by the same characteristics as electrical anisotropy, then the Packsaddle Schist should exhibit electrical anisotropy with principal directions parallel and perpendicular to the foliation. Differences of principal components could exist within the plane of foliation if the minerals exhibit a pronounced lineation. The latter does not appear prominent in the rocks at the study site.

Compositional banding, also known as a gneissic texture, is the presence of alternating layers of felsic-rich and mafic-rich minerals roughly parallel to foliation. In the absence of mineral foliation, compositional banding can produce a bulk transverse anisotropy even though each layer is isotropic but of differing electrical properties.

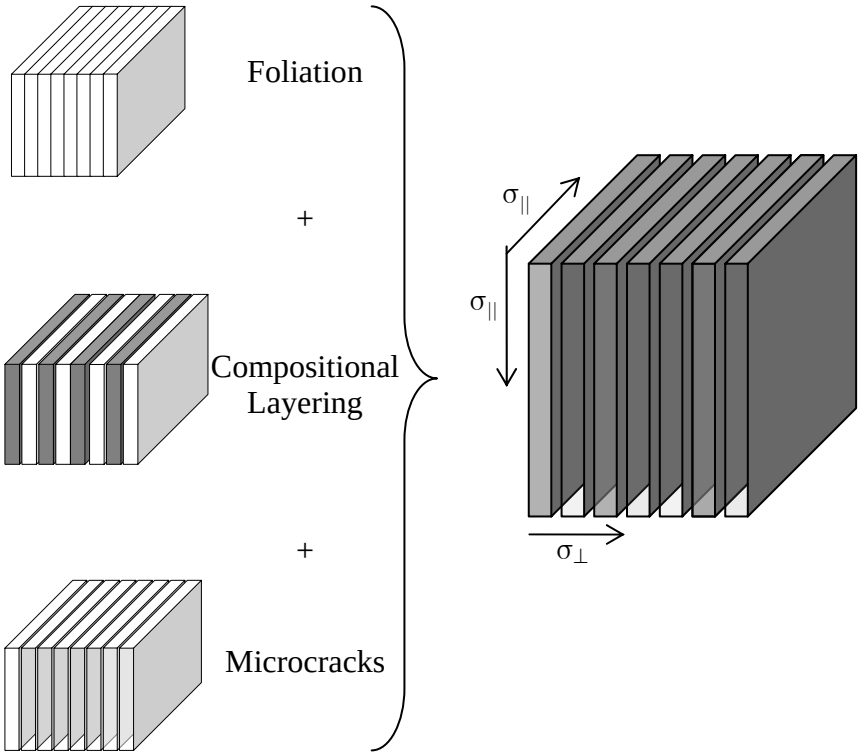

Figure 8. Factors contributing to anisotropy in metamorphic rocks. They are all related to the unequal stresses directed mainly horizontal during the process of metamorphism. (a) Foliation is the parallel alignment of minerals. (b) Compositional banding is the alternating layers of mafic and felsic minerals. This is also known as a gneissic texture. (c) Microcracks form along planes of weakness, usually parallel to foliation, when a rock experiences a decrease in pressure. (d) Any combination of these factors may contribute to the anisotropic behavior of a metamorphic rock.

Therefore, the electrical anisotropy produced by compositional layering evident in the Packsaddle Schist adds constructively to the electrical anisotropy due to mineral foliation.

Microcracks commonly are preferentially located a grain boundaries. Thus if mineral grains are elongate or platy and exhibit a preferred orientation fabric as in a foliated metamorphic rock, then microcracks will exhibit a synthetic fabric with the mineral grain fabric. The preferred orientation of microcracks will produce anisotropy of the fluid permeability tensor. Surfaces of minerals and the pore space and pore fluid strongly influence electrical conductivity of a rock. Consequently this component of electrical conductivity closely mirrors the fluid permeability attributes in rocks. Since electrical conductivity is closely linked to fluid flow, grain boundary cracks produce a higher electrical conductivity along their orientation than across, assuming the grain boundaries exhibit a preferred orientation. Therefore, grain boundary cracks are hypothesized to enhance the electrical anisotropy, with the maximum principal component oriented parallel to foliation.

Weathering can constructively or destructively affect the electrical anisotropy of a rock mass. In general, the degree of weathering decreases with depth. Weathering at the survey site could increase the size and number of the grain boundary cracks, thus increasing permeability, and hence increasing electrical conductivity parallel to foliation. In addition, thin films of clay minerals deposited or formed within the grain boundary cracks can increase electrical conductivity because of surface chemistry. However, the inclusion of clay may decrease permeability, therefore decreasing electrical conductivity. Weathering could also randomly break the rocks creating new cracks oriented oblique or perpendicular to the foliation, hence possibly reducing the effects of microcrack-related

anisotropy. Therefore, weathering could help or hinder the anisotropic signature along foliation in this case. It could also produce systematic vertical variation of electrical properties, thus resulting in vertical heterogeneity. This would negate a homogeneous half-space model, but a multiple horizontal layer may be appropriate.

At a large scale, macrocracks or "joints" are present in the region and must be considered when determining the cause of anisotropy. The electrical conductivity along macrocracks is assumed to be higher than across the macrocracks due to higher permeability parallel to the microcracks. For macrocracks to produce an anisotropic effect, the macrocracks must have a similar orientation over some aerial extent, be sufficiently closely spaced as to cause a "bulk response" to be constrained within the survey dimensions, and numerous enough to contribute to anisotropy. The anisotropy of the macrocracks will most likely not be parallel to foliation and thus add a directionality difference to foliation-related anisotropy. This could reduce the observed anisotropic bulk response unless one strongly dominates the effect of the other. Degree of water saturation and clay content of macrocracks also will contribute to the effect on electrical conductivity.

Detecting anisotropy in metamorphic rocks using TDEM requires an understanding of what properties are being measured and the control of these parameters in metamorphic rocks. The contributions of foliation, compositional banding, grain boundary cracks, weathering, and systematic fracture systems exist at the study site. TDEM, DC resistivity and seismic methods used at the study site each detect anisotropy oriented in the same direction, indicating that the cause(s) of anisotropy exhibit both elastic and electric anisotropy.

TIME-DOMAIN ELECTROMAGNETIC SURVEY

Overview

Eight azimuthal, time-domain, controlled source, electromagnetic surveys were conducted at 5 locations (Figure 9) within the study site to detect subsurface anisotropy. In theory, if the medium possesses a vertical, transverse electrical anisotropy, then EM measurements vary with azimuth of the transmitter and receiver with respect to the orientation of the principal component of anisotropy, exhibiting a bi-lobate pattern when plotted in polar format (Figure 10) [*al-Garni and Everett*, 2003].

The study area is approximately 300 m^2 in size and is thought to exhibit transverse electrical anisotropy due to multiple characteristics of the metamorphic Packsaddle Schist as outlined in the previous section. A Geonics PROTEM47 instrument was the time-domain EM system used for this study. This device measures the voltage raised in the RX by transient eddy current decay within the subsurface which is induced by a controlled source. The voltage waveform generated in the RX is controlled by the conductive behavior of the medium. Conductive media respond initially with a small amplitude signal that decays relatively slowly, whereas resistive targets have a high initial amplitude signal that decays rapidly (Figure 11). To resolve the nature of transient decays, voltage measurements are made at 20 logarithmically spaced, sample times ("time gates") ranging from 6.81 to 701 μs (Table 1). The gates are concentrated at early time, when the most rapid decay occurs. The depth of investigation of the system is

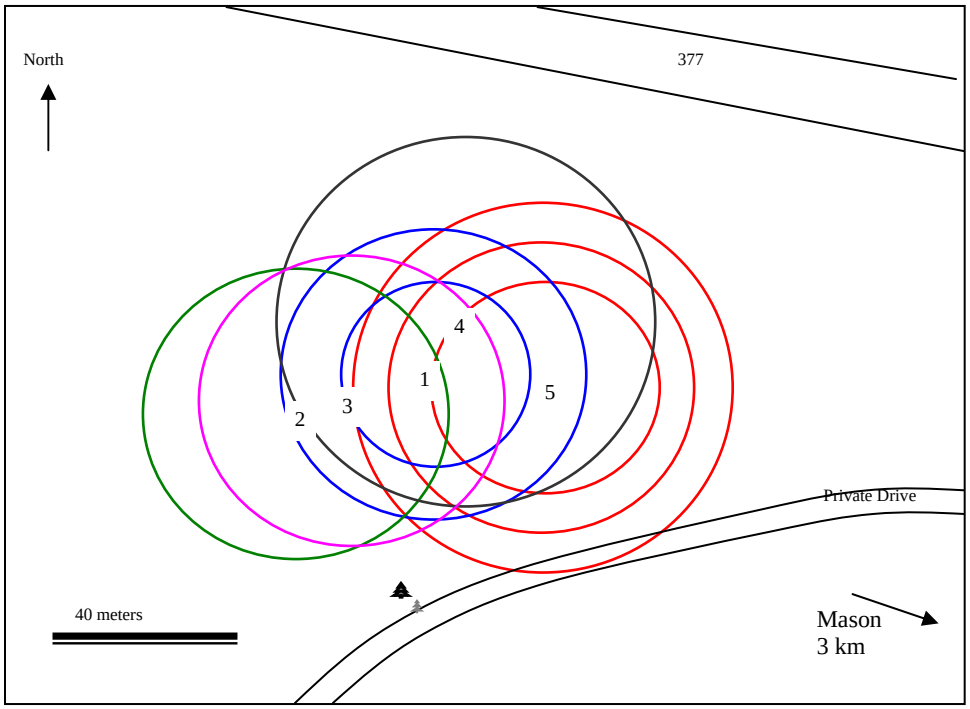

Figure 9. Survey map of the field site. The numbers indicate the 5 respective transmitter locations for the electromagnetic surveys. The eight circular lines indicate the path of receiver locations of each survey conducted. Blue indicates Location 1, Surveys 1 and 2; Green indicates Location 2, Survey 3; Pink indicates Location 3, Survey 4; Gray indicates Location 4, Survey 5; Red indicates Location 5, Surveys 6, 7, and 8.

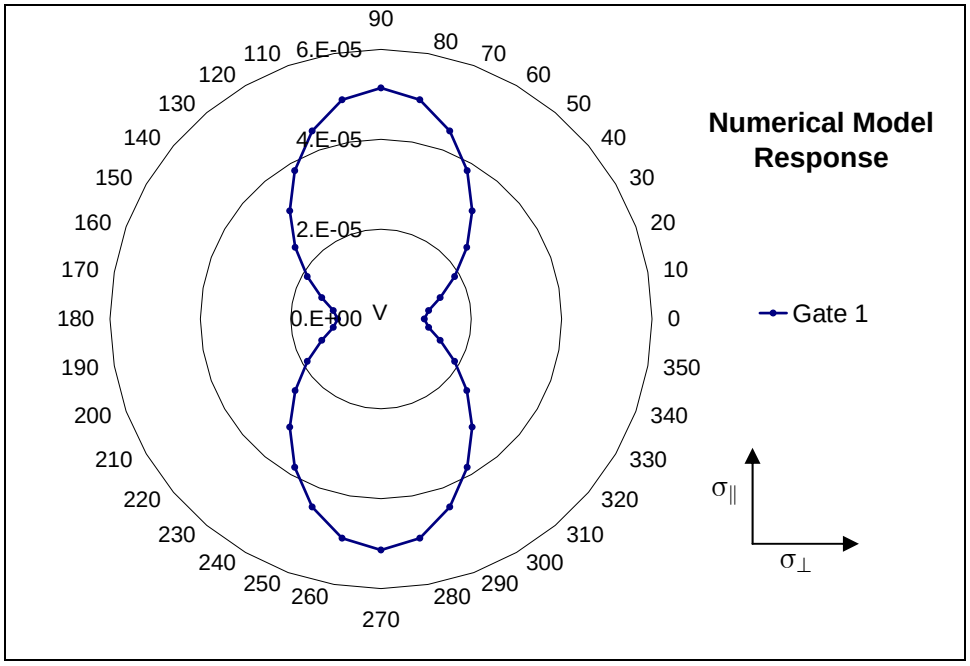

Figure 10. Theoretical two-lobed TDEM response. This is a polar plot of the theoretical voltage [Volts] generated in the RX as a function of azimuth where $\varphi = 0$ corresponds to the direction normal to the strike of anisotropy and $\varphi = 90$ corresponds to the direction parallel to the strike of anisotropy. This plot can be visualized as a plan view map of voltage above an anisotropic half-space. Notice the distinctive two lobed shape that stretches out in the direction along the strike of anisotropy, $\sigma_{\|}$, and pinches inward in the direction across the strike of anisotropy, $\sigma_{\perp}$. This is characteristic of a TDEM response above a vertical transversely anisotropic half-space. Numerical calculations derived this response as discussed in the Forward Modeling chapter.

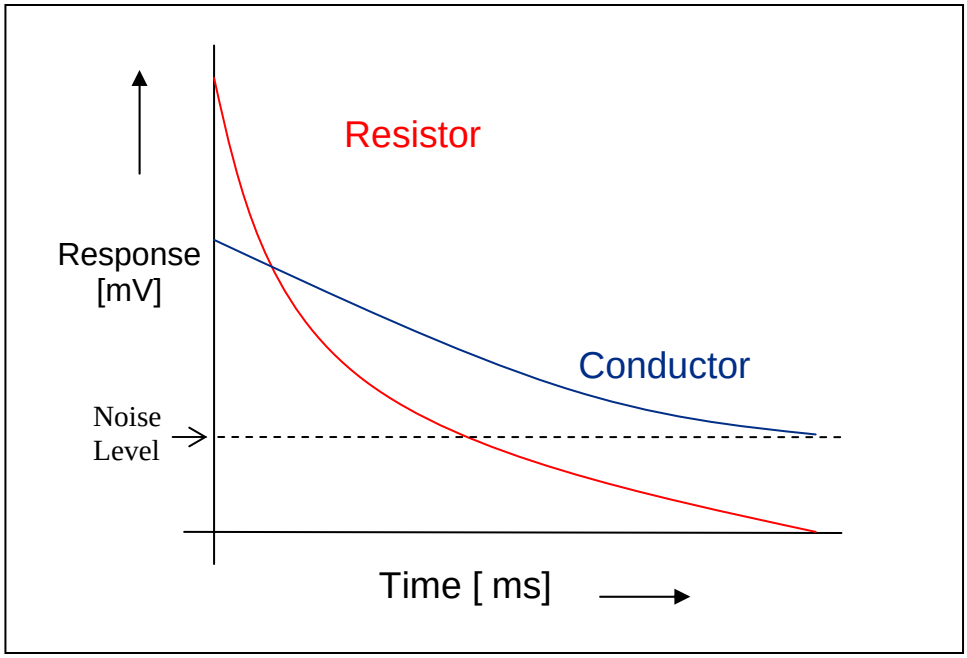

Figure 11. TDEM Response: Resistor vs. Conductor. Higher resistivity (red) displays a higher initial response, but decays quickly to the noise level. Higher conductivities (blue) display a lower initial response but persist longer.

Table 1. Geonics PROTEM47 system time gates. List of the 20 logarithmically spaced time gates and the corresponding times for the Geonics PROTEM 47 system. For this study we will focus on the first five time gates.

Gate #	*Time (sec)*	*Gate #*	*Time (sec)*
1	6.850E-06	11	8.380E-05
2	8.950E-06	12	1.046E-04
3	1.208E-05	13	1.356E-04
4	1.572E-05	14	1.723E-04
5	2.000E-05	15	2.149E-04
6	2.617E-05	16	2.750E-04
7	3.340E-05	17	3.490E-04
8	4.210E-05	18	4.360E-04
9	5.410E-05	19	5.550E-04
10	6.820E-05	20	7.010E-04

governed by the signal to noise ratio, which in turn is determined by the transmitter moment, receiver sensitivity, and the time gate distribution. The measurement system consists of a single turn transmitter loop of 5 m radius and a rigid multi-turn receiver loop, which are independent of each other. In order to assess potential transverse, electrical anisotropy the transmitter loop was placed at a fixed central location with the receiver loop moved progressively 360º around a circle of fixed radius. A 360º rotation permits a complete azimuthal characterization to explore the symmetry of the anisotropic behavior [*Watson and Barker*, 1999]. If the medium exhibits a vertical transverse anisotropy, then the response will exhibit two, mutually perpendicular mirror planes of symmetry. Each 360º rotation of the RX is termed a "survey" in this text and is conducted at different radii ranging from 25 m to 50 m. The locations of the eight different surveys are indicated in Figure 9 and will be referred to as "locations" in this text. By changing the location of the transmitter loop, it is possible to map the lateral extent of the subsurface anisotropy. Different radii of the surveys assess the variation of electrical properties and potential anisotropy at different depths.

Polar plots of voltage at the first five time gates as a function of azimuth were made to aid in the analysis and interpretation of the data. Azimuth zero corresponds to north on the polar plots shown subsequently. Four statistical measures were used to analyze azimuthal data for anisotropic behavior. These measurements were developed by *Busby* [2002] for direct current resistivity data. These measures have herein been adapted to TDEM based on the assumption that voltage readings in EM systems are proportional to the apparent conductivity of the subsurface.

Theory of Time-Domain Electromagnetics

Electric and magnetic field components induced within the subsurface are measured by EM methods. In TDEM systems the controlled source waveform is transient, meaning it varies with time. The Geonics TEM47 system includes a transmitter loop (TX) and a receiver loop (RX) that are independent of each other, and situated at the Earth's surface. A transient current flows through the TX as a slow rise, followed by a steady ON, followed by a sudden ramp OFF (Figure 12a) [*McNeill*, 1980].

According to Ampere's Law

$$\nabla \times \vec{B} = \mu_o \sigma \vec{E} + \vec{J}_s, \tag{1}$$

an electric current $\vec{J} = \sigma \vec{E}$ generates a magnetic field $\vec{B}$ where μ_0 is the magnetic permeability of free space [H/m] and σ is electric conductivity [S/m]. Therefore the transient current $\vec{J}_s(t)$ in the TX generates a primary magnetic flux in the vicinity of the loop. As this magnetic flux diffuses through the Earth, it generates an electromotive force (emf) within the subsurface (Figure 12b), as defined by Faraday's Law:

$$\nabla \times \vec{E} = -i\omega \partial \vec{B} \big/ \partial t \,. \tag{2}$$

Faraday's Law states that changing magnetic flux $\vec{B}$ of frequency ω over time t through a circuit establishes an emf which, if the circuit is conductive, causes a current to flow. Due to the conductive nature of the Earth, the emf induces currents within the subsurface according to the local conductivity. In an idealized homogeneous Earth, the induced currents move downward and outward with a decreasing velocity and diminishing amplitude, resembling a system of 'smoke rings' [*Nabighian*, 1979]. According to

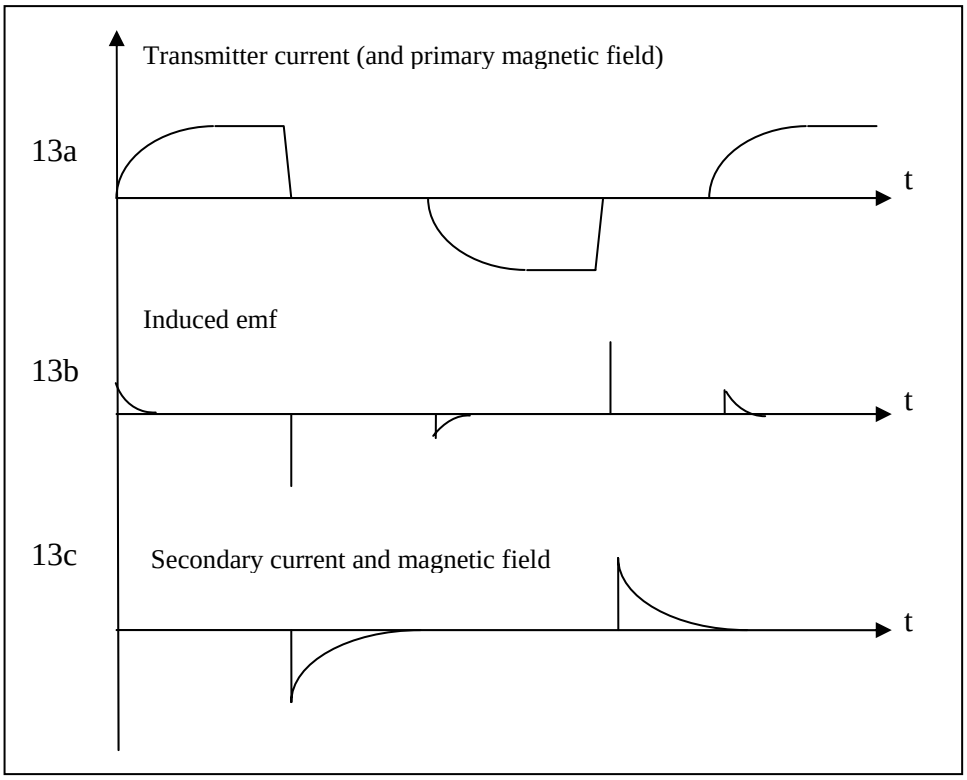

Figure 12. Waveforms of a time-domain electromagnetic system. (a) A transient current flows through the transmitter loop as a slow rise, followed by a steady ON, followed by a sudden ramp OFF, (b) electromotive forces are induced in the subsurface by the primary magnetic field produced by the transmitter current and (c) a current is raised in the receiver loop by the secondary magnetic field produced by current decay within the subsurface [*McNeil*, 1980].

McNeill [1980] the currents flowing in the subsurface exhibit a transient decay that is characteristic of conductor size, shape, and conductivity. In turn, the subsurface currents create a secondary magnetic field following Ampere's law (Equation 1). The RX coil detects the time-rate-of-change of the secondary magnetic field and according to Faraday's law (Equation 2) a proportional emf (voltage) develops in the RX loop (Figure 12c). Information from the voltage raised in the RX loop can be used to interpret the subsurface electrical properties.

In transient EM, subsurface electrical conductivity is determined by the rate at which currents decay. Therefore, the EM response is sampled at multiple times. The sample time, or "gates" are concentrated at early time to detect the initial rapid current decay. At later time, magnetic flux through the RX loop changes direction. This zero crossing time can be utilized to determine the apparent conductivity of the subsurface in a homogeneous isotropic half-space:

$$\tau \sim \frac{\mu_0 \sigma \mathrm{L}^2}{10}, \tag{3}$$

where τ is the zero crossing time, μ_0 is the magnetic permeability of free space, σ is electrical conductivity, and L is the TX-RX separation distance. The early-time ($t << \tau$) response is greater in resistive bodies than in conductive bodies. However, the response decays quicker in resistors, so currents persist longer in conductive bodies (Figure 11). Once the driving forces of electromagnetic induction are understood, it is important to see how subsurface anisotropy affects the electromagnetic response.

Paradox of Anisotropy

Al-Garni and Everett [2003] derived an analytic solution in the frequency domain for the electromagnetic loop-loop response of an idealized set of vertical fractures that can produce vertically transverse anisotropic behavior (Figure 1). The electrical conductivity σ was assumed to be a tensor of the form:

$$\sigma = \mathrm{diag}(\sigma_{\perp},\sigma_{||},\sigma_{||}). \quad (4)$$

In the subsurface model, the along-strike electrical conductivity $\sigma_{||}$ is assumed to be greater than the across-strike electrical conductivity, $\sigma_{\perp}$. The electromagnetic prospecting system is modeled as a stationary transmitter loop with a receiver loop moved azimuthally at a fixed radius L from the transmitter. Results from calculations (Figure 2) indicate that apparent conductivity is larger at azimuth ϕ=0º (transmitter and receiver aligned across fractures) than at azimuth ϕ=90º (transmitter and receiver aligned along fractures). This suggests that the across-strike conductivity, $\sigma_{\perp}$, is larger than the along-strike conductivity, $\sigma_{||}$. In actuality, the reverse is true, giving rise to the "paradox of electrical anisotropy." Al-Garni and Everett resolve the paradox by recognizing that the response is actually controlled by the conductivity in the direction of the local-induced current flow beneath the receiver loop (Figure 13). The numerical modeling from al-Garni and Everett (2003) will be used but re-cast in the time-domain to model the experimental results obtained over the Packsaddle Schist.

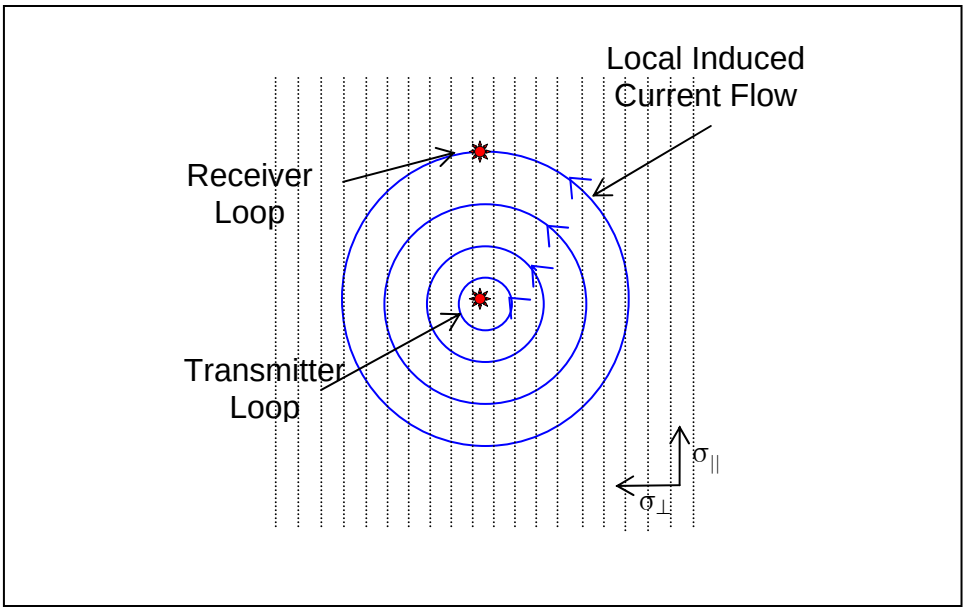

Figure 13. Illustration of an EM paradox of anisotropy. Actual electrical conductivity is greater in the along strike direction, $\sigma_{||}$, than in the across strike direction, $\sigma_{\perp}$. Apparent electrical conductivity is higher across strike than along strike due to local current flows (blue) beneath the receiver loop.

TEM47 Results

Eight time-domain, controlled-source EM, azimuthal surveys were conducted during this study. The distribution of the five transmitter locations for the surveys is shown in Figure 9. TX-RX separations for the surveys range from 25 m to 50m. At Location 1, a 25 m and 40 m survey were conducted. 40 m surveys were conducted at Locations 2, and 3. Location 4 was surveyed using a 50 m TX-RX separation, and Location 5 was surveyed using 3 separations of 30, 40, and 50 m. Polar plots of the voltage induced in the RX for each of the surveys are shown in Figures 14-21. Note that φ=0 corresponds to north and that the plots are displayed using different scales of millivolts. Large differences in scales between surveys are a result of different gain settings, RX-TX separations, and attributes of the EM system. For the present study, azimuthal variations of measured voltages within a given survey will be considered. Differences between voltages measured at different survey locations will not be considered.

Polar plots of voltage data for the eight surveys include data from the first five time gates. The first time gate represents the largest induced voltage and varies most with azimuth resulting in a two-lobed theoretical response that can be approximately described by the following equation

$$V = \sqrt{\left(V_{\max}\cos(\varphi)\right)^2 + \left(V_{\min}\sin(\varphi)\right)^2} \qquad (5)$$

where V is the voltage raised in the TX loop and φ is the azimuth of the TX-RX orientation relative to the strike of foliation. Theory predicts a two-lobed shape if the medium has vertical transverse electrical anisotropy, where the maximum principal axis is oriented parallel to foliation [*al-Garni and Everett*, 2003]. Each of the azimuthal

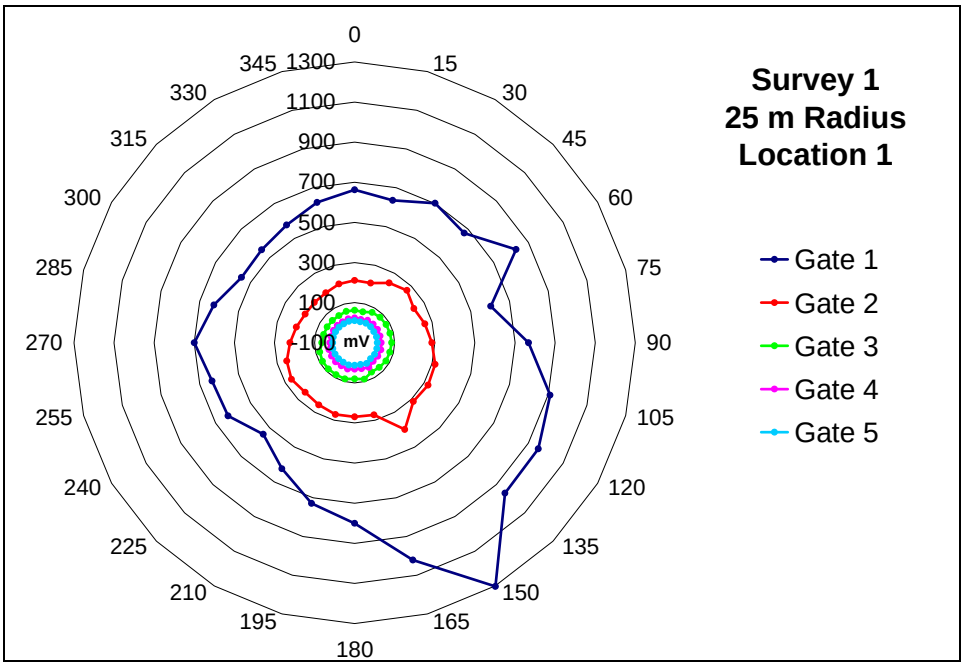

Figure 14. TDEM Survey 1, Location 1 data. This survey was conducted with a 25 meter TX-RX separation. Voltage readings [mV] in the RX loop are plotted as a function of azimuth from north (0º) every 15º. This plot is indicative of high voltage readings due to the small TX-RX separation and illustrates only a single mirror plane of symmetry for early time. It does not correlate well with the expected two-lobed response in Figure 11. However, it does show a maximum principal axis greater than the minimum principal axis. The measured strike of foliation of the Packsaddle Schist is 146º.

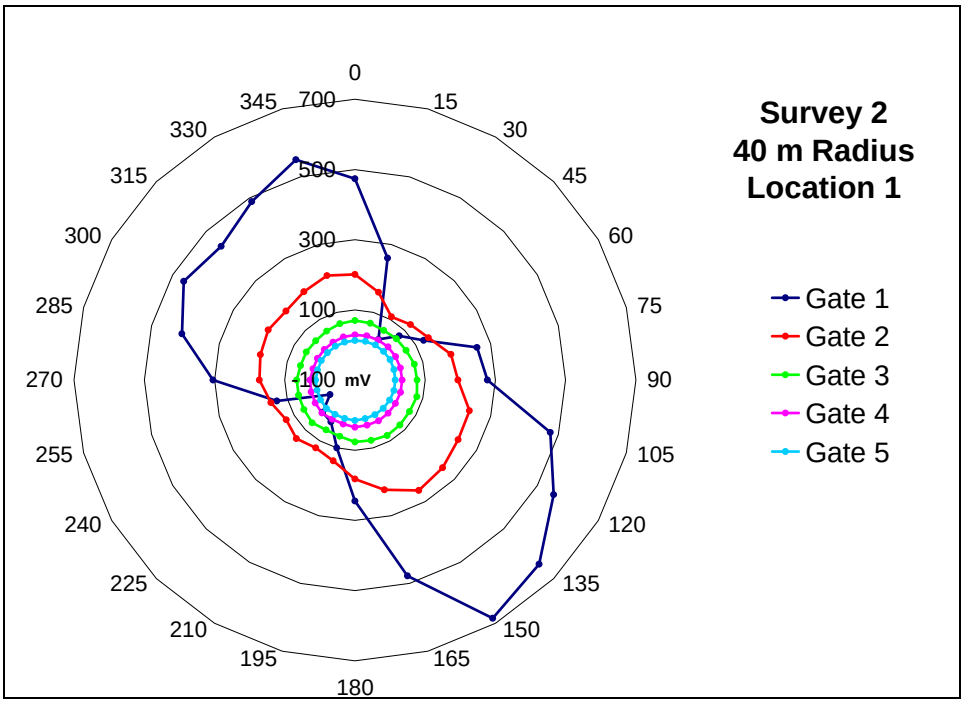

Figure 15. TDEM Survey 2, Location 1 data. This survey was conducted with a 40 meter TX-RX separation. Voltage readings [mV] in the RX loop are plotted as a function of azimuth from north (0º) every 15º. This plot correlates very well (R^2 = 93%) with the expected two-lobed response for the first time gate (Figure 11) exhibiting two perpendicular mirror planes of symmetry. The measured strike of foliation of the Packsaddle Schist is 146º.

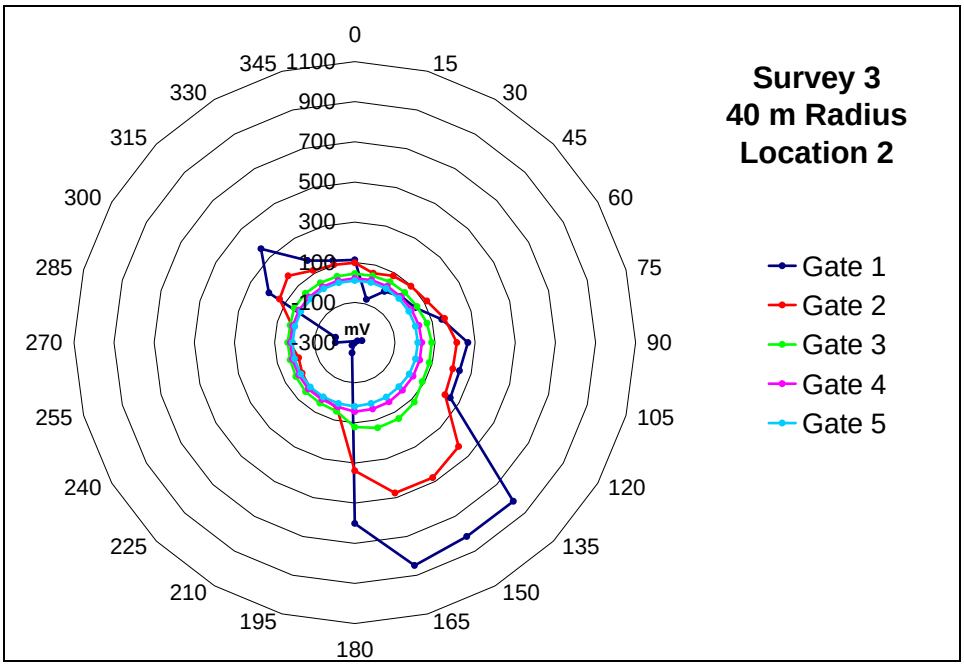

Figure 16. TDEM Survey 3, Location 2 data. This survey was conducted with a 40 meter TX-RX separation. Voltage readings [mV] in the RX loop are plotted as a function of azimuth from north (0º) every 15º. This plot illustrates asymmetry indicating spatial variability or heterogeneities. It correlates closely with the expected two-lobed response in Figure 11, showing a maximum principal axis "stretched out" and a minimum principal axis that "pinches in". The measured strike of foliation of the Packsaddle Schist is 146º.

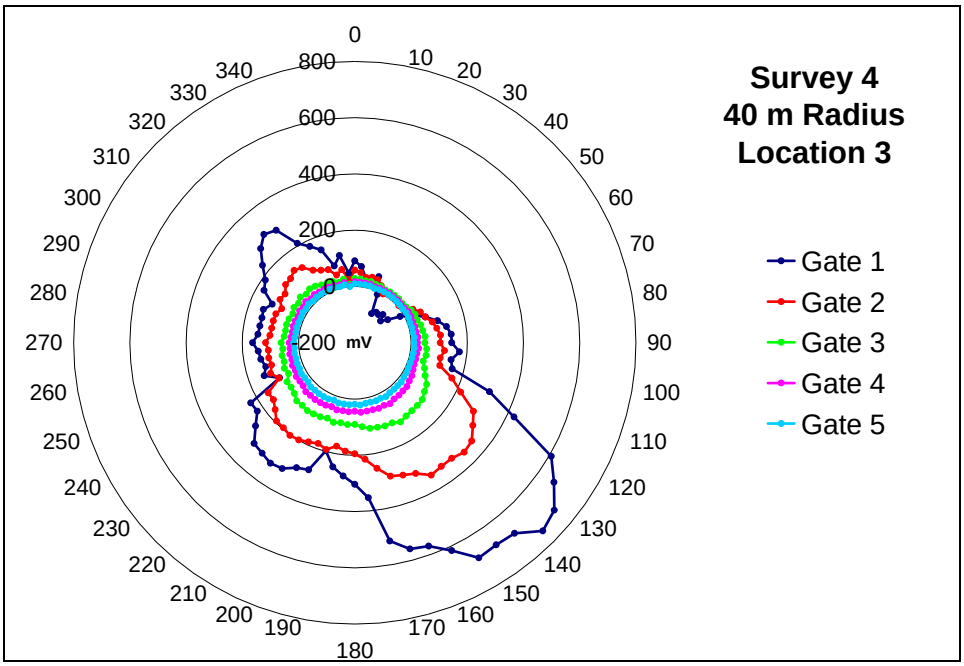

Figure 17. TDEM Survey 4, Location 3 data. This survey was conducted with a 40 meter TX-RX separation. Voltage readings [mV] in the RX loop are plotted as a function of azimuth from north (0º) every 10º. The measured strike of foliation of the Packsaddle Schist is 146º.

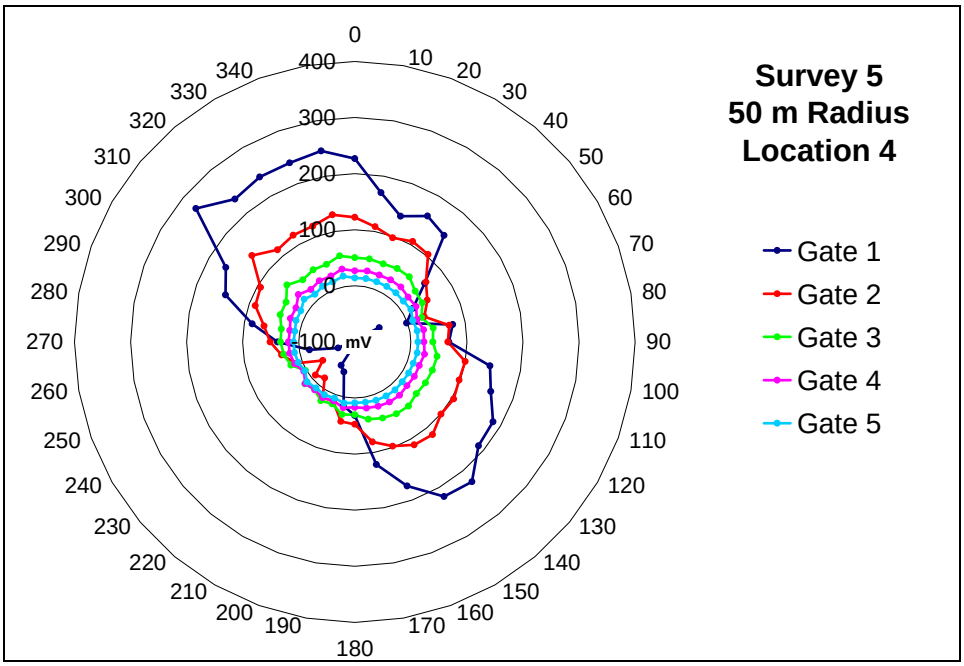

Figure 18. TDEM Survey 5, Location 4 data. This survey was conducted with a 50 meter TX-RX separation. Voltage readings [mV] in the RX loop are plotted as a function of azimuth from north (0º) every 5º. The above plot correlates very well with the expected two-lobed TDEM response (Figure 11), exhibiting one mirror plane of symmetry. The measured strike of foliation of the Packsaddle Schist is 146º.

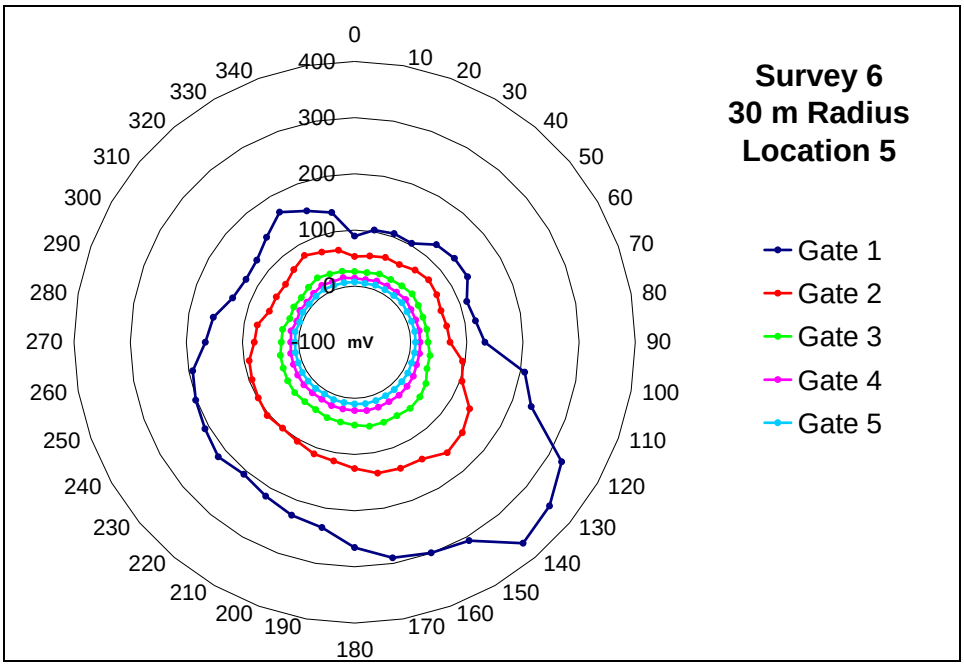

Figure 19. TDEM Survey 6, Location 5 data. This survey was conducted with a 30 meter TX-RX separation. Voltage readings [mV] in the RX loop are plotted as a function of azimuth from north (0º) every 10º. This plot is approximately circular in shape with slight asymmetry stretching the voltages out in the northwest-southeast directions. The measured strike of foliation of the Packsaddle Schist is 146º.

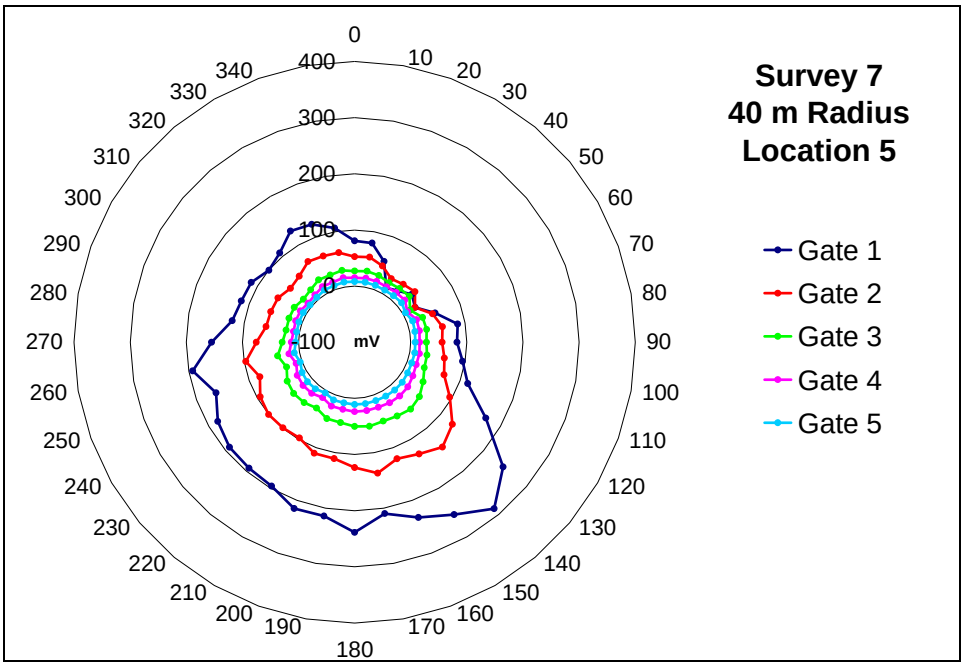

Figure 20. TDEM Survey 7, Location 5 data. This survey was conducted with a 40 meter TX-RX separation at the same location as Survey 6. Voltage readings [mV] in the RX loop are plotted as a function of azimuth from north (0º) every 10º. This plot is approximately circular in shape with slight asymmetry stretching the voltages out in the northwest-southeast directions, showing a slight increase in along-strike conductivity. The measured strike of foliation of the Packsaddle Schist is 146º.

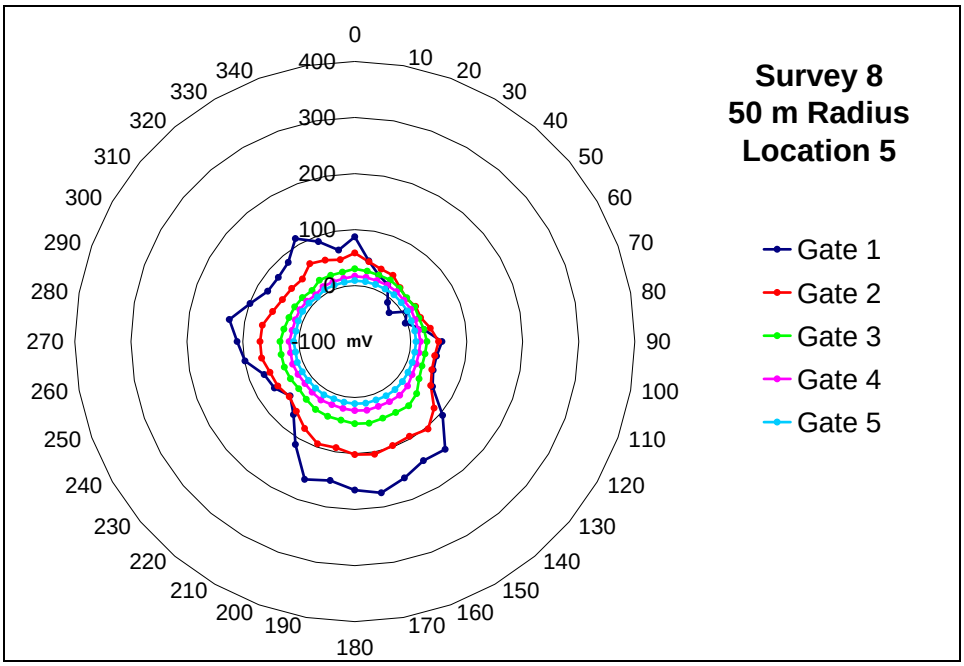

Figure 21. TDEM Survey 8, Location 5 data. This survey was conducted with a 50 meter TX-RX separation at the same location as Surveys 6 and 7. Voltage readings [mV] in the RX loop are plotted as a function of azimuth from north (0º) every 10º. This plot shows a two-lobed shape unlike Figures 19 and 20. The larger TX-RX separation of this survey compared to the previous surveys allows deeper penetration. The "lobes" of this plot are again asymmetric with the bottom lobe oriented in a different direction than the top lobe, indicating spatial variability at the field site. The measured strike of foliation of the Packsaddle Schist is 146º.

TDEM surveys shows larger Gate 1 voltage in the northwest-southeast direction. Transient EM theory has established that early-time voltage is higher in resistors than in conductors (Figure 11), indicating higher resistivity (lower conductivity) in the northwest-southeast direction. However, the paradox of anisotropy in electromagnetic induction indicates the reverse is actually true [*al-Garni and Everett*, 2003]. Therefore, higher conductivity is in the northwest-southeast direction, as expected by alignment along the measured strike of foliation. Each progressive time gate becomes more circular until the response becomes very small by gate 5, which is expected in transient electromagnetics over resistive crystalline rocks. The late-time tendency to a circular response is due to an averaging effect of the along- and across-strike conductivities by deeper subsurface currents that are detected by the RX. Figure 22 compares the voltage response over time at Survey 6 (Location 5, 30 m radius). At early times (gates 1-5) the magnitude of the response is significant enough to provide information about the subsurface. However, at intermediate times (gates 6-10), late time (gates 11-15), and very late time (gates 15-20), no azimuthal variation is detected at the noise level. This indicates that useful information about anisotropy of the subsurface anisotropy is contained within the first five time gates. The rapid decay to the noise level is expected for this study because the resistive nature of crystalline rocks cause eddy currents to decay quickly.

Further interpretation and analysis of the azimuthal plots requires statistical confirmation that anisotropy is present. The paper by *Busby* [2000] developed four statistical measures to analyze direct current resistivity data for anisotropy by

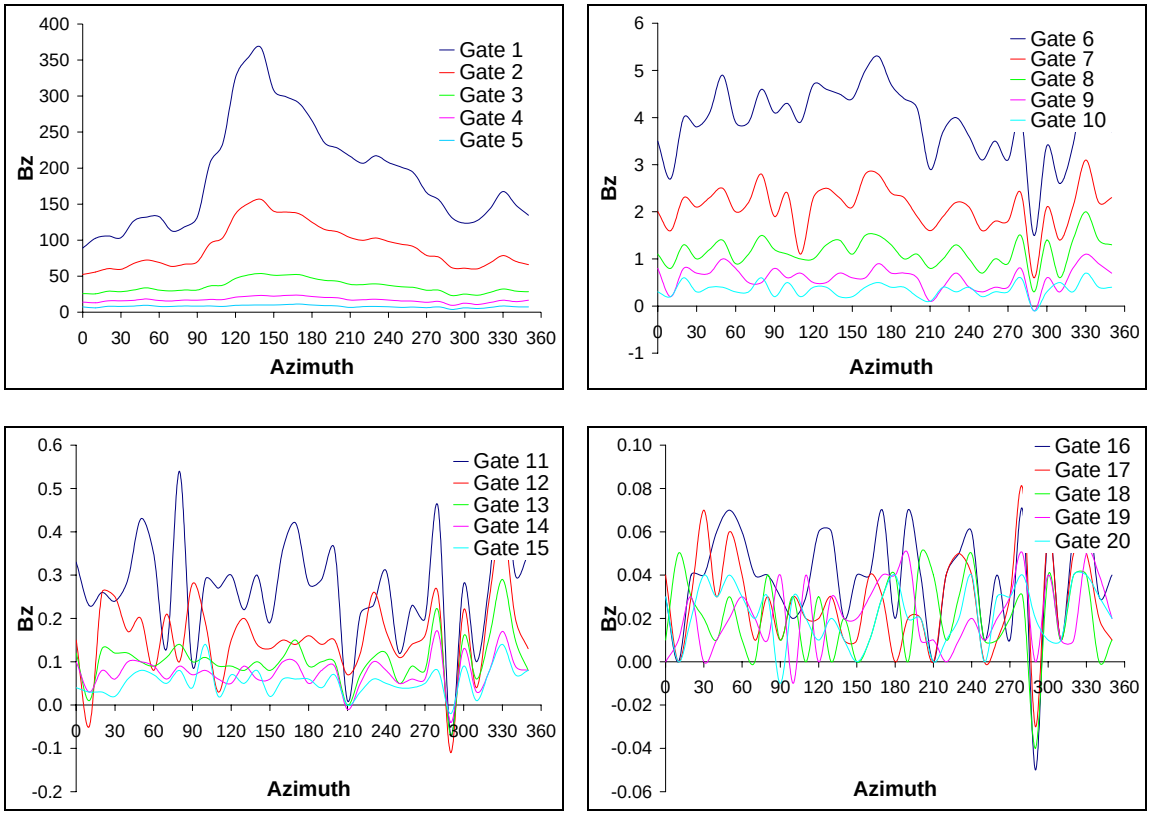

Figure 22. Response over time for Survey 6 (30 m radius), Location 5. (a) Early-time (Gates 1-5) response indicates that the first 5 time gates provide useful information about the subsurface to signify an anisotropic response (b) mid-time (Gates 6-10) responses have decayed quickly (2 orders of magnitude) and provide little information about the subsurface that indicates anisotropy (c) late-time responses (Gates 11-15) have decayed 3 orders of magnitude lower than the initial response which is the electromagnetic noise level and (d) very-late time response (Gates 16-20) decays 4 orders of magnitude and fluctuates around zero at the noise level.

(1) determining if the subsurface is sufficiently homogeneous to detect anisotropy; (2) determining if the azimuthal variations indicate anisotropy; (3) quantitatively describing the anisotropy if 1 and 2 are satisfied; and (4) determining the cause of anisotropy. The proportionality between apparent resistivity and voltage responses in TDEM allows these criteria to be applied to this study.

1 *Is the subsurface sufficiently homogeneous to detect anisotropy*?

Determining the degree of heterogeneity relative to the scale of measurements is necessary in order to quantitatively determine if the effects of anisotropy are greater than those of the inhomogeneities present. If the data prove the site is sufficiently homogeneous, then interpretation of anisotropy can be made confidently. In direct current resistivity, a homogeneity index is defined by dividing the divergence of azimuthal measurements from a circular pattern by the dispersion of measurements using the equation

$$\frac{\sigma\left(\rho_{D1,D2}\right)}{\sigma\left(\left|\rho_{D1}-\rho_{D2}\right|\right)}. \tag{6}$$

where σ is standard deviation and ρ is apparent resistivity. The same concept can be applied to electromagnetics because the voltage response can be interpreted as an apparent conductivity [*al-Garni and Everett*, 2003]. Therefore, a measure of anisotropy is found by dividing the standard deviation of the average voltage response of the eight surveys by the standard deviation of the average difference between each survey value and the average value. A value of 1.18 is obtained, indicating variation due to anisotropy is greater than that due to inhomogeneity. Values above 1.39 are considered to strongly

support the assumption of homogeneity according to empirical data in the paper by *Busby* [2000]. Therefore, our data implies less strong support for assumed homogeneity, but further interpretation can proceed with caution.

2 Are the azimuthal variations significant enough to indicate anisotropy?

Once the subsurface is determined to be sufficiently homogeneous, the data must be analyzed to determine that the response is due to anisotropic effects. The statistic R^2 is found by subtracting the variance, σ^2, between the best-fit contour for vertical transverse anisotropy (Equation 5) and data from the variance of the data and dividing the result by the variance of the data.

$$R^2 = \frac{(\sigma^2_{data} - \sigma^2_{contour-data})}{\sigma^2_{data}} \times 100\% \quad (7)$$

This value indicates the percentage of variance from a circular model. A value of 1 (100%) indicates a perfect fit to the contour and values from 0.1 to 0.2 (~10-20%) indicate isotropy [*Busby*, 2000]. The eight survey values (Table 2) range from 52% to 93%, with the average of 82% for the first time gate. The degree of anisotropy depends on the transmitter-receiver loop separations due to the behavior of electromagnetic induction and the geology at the field site. Despite these limitations, the values of percent anisotropy do sufficiently indicate the presence of anisotropy in each of the surveys.

Table 2. Quantitative measures of anisotropy for the 8 TDEM surveys. Strike is the direction of the maximum principal axis of the best fitting contour (Equation 5), λ is the ration of the maximum and minimum principal axes for the data and the best fitting contour, R^2 is the reduction in variance between the data and the best fitting contour, and the Average Value is the average voltage in Ωm.

Survey	*Location*	*Radius*	*Axis Strike [degrees]*	*Time Gate*	*Average Value [Ωm]*	R^2	*Percentage Anisotropy*	λ_{data}	$\lambda_{contour}$
1	1	25 m	140	1	734.10	66%	± 10%	1.55	1.10
				2	184.10	71%	± 16%	1.47	1.17
				3	73.80	76%	± 7%	1.25	1.07
				4	5.76	55%	± 8%	1.45	1.08
				5	2.62	53%	± 11%	1.61	1.12
2	1	40 m	138	1	313.23	93%	± 78%	6.16	10.49
				2	178.79	54%	± 36%	1.56	1.43
				3	69.76	82%	± 3%	1.20	1.04
				4	3.66	75%	± 8%	1.22	1.08
				5	2.77	88%	± 11%	1.25	1.12
3	2	40 m	150	1	127.21	52%	± 41%	1.59	1.52
				2	150.03	42%	± 82%	7.08	4.81
				3	65.10	22%	± 3%	2.03	1.04
				4	27.71	38%	± 8%	1.50	1.08
				5	11.81	48%	± 11%	1.46	1.12
4	3	40 m	140	1	227.70	94%	± 83%	3.04	2.57
				2	137.55	89%	± 57%	22.36	1.83
				3	61.21	96%	± 84%	3.71	2.65
				4	29.28	96%	± 9%	4.17	1.10
				5	13.57	92%	± 3%	14.97	0.97
5	4	50 m	137	1	100.96	84%	± 74%	1.34	4.47
				2	73.78	85%	± 72%	2.02	3.61
				3	38.52	77%	± 25%	6.02	1.29
				4	21.58	79%	± 17%	2.55	1.19
				5	11.54	76%	± 17%	2.52	1.18
6	5	30 m	137	1	189.21	83%	± 21%	2.03	1.24
				2	90.59	82%	± 11%	1.73	1.12
				3	35.76	75%	± 14%	1.53	1.15
				4	17.12	79%	± 15%	1.58	1.16
				5	8.11	63%	± 7%	1.68	1.07
7	5	40 m	142	1	138.48	90%	± 27%	4.89	1.33
				2	77.38	90%	± 19%	2.45	1.21
				3	16.73	80%	± 13%	1.96	1.14
				4	16.73	81%	± 19%	1.74	1.21
				5	8.03	66%	± 25%	1.91	1.29
8	5	50 m	149	1	81.10	90%	± 57%	2.94	2.08
				2	60.09	89%	± 25%	2.28	1.29
				3	31.76	82%	± 11%	1.62	1.11
				4	17.24	72%	± 26%	1.73	1.31
				5	8.71	68%	± 20%	1.82	1.22

3 Can the anisotropy be described quantitatively?

Three elements are necessary to describe anisotropy. First is the orientation of the maximum principal axis of the best fitting contour for each survey (Figure 23 and Table 2). An average orientation of the principal axis is 137º, which correlates well (within 10º) to the measured strike of foliation of 146º. The second is a quantity used to describe the anisotropy. The coefficient of anisotropy, λ, is a parameter indicated by the ratio of the maximum and minimum principal axes of the best fit contour. Values of $\lambda > 1.0$ indicate anisotropy. For each survey, the coefficient of anisotropy indicates some degree of anisotropy is present, with the average value of 2.83 well above homogeneity of 1.0. A third quantity indicates the percent variation from the average for each survey using the equation

$$\pm\frac{1}{2}\left[\frac{\left(V_{\max}-V_{\min}\right)}{V_{avg}}\right]100\% . \qquad (8)$$

This value is found by subtracting the minimum voltage of the best fitting contour from the maximum voltage of the best fitting contour and dividing the difference by the average of the two. The average percent anisotropy for the eight surveys is 50%, with the smallest values correlating to smaller TX-RX separations.

4 What is the cause of anisotropy?

The Packsaddle Schist in the subsurface suggests that the cause of electrical anisotropy is due to foliated metamorphic rock. Foliation creates micro-scale anisotropy with mineral foliation, mineral lamination, compositional banding, and grain boundary cracks (Figure

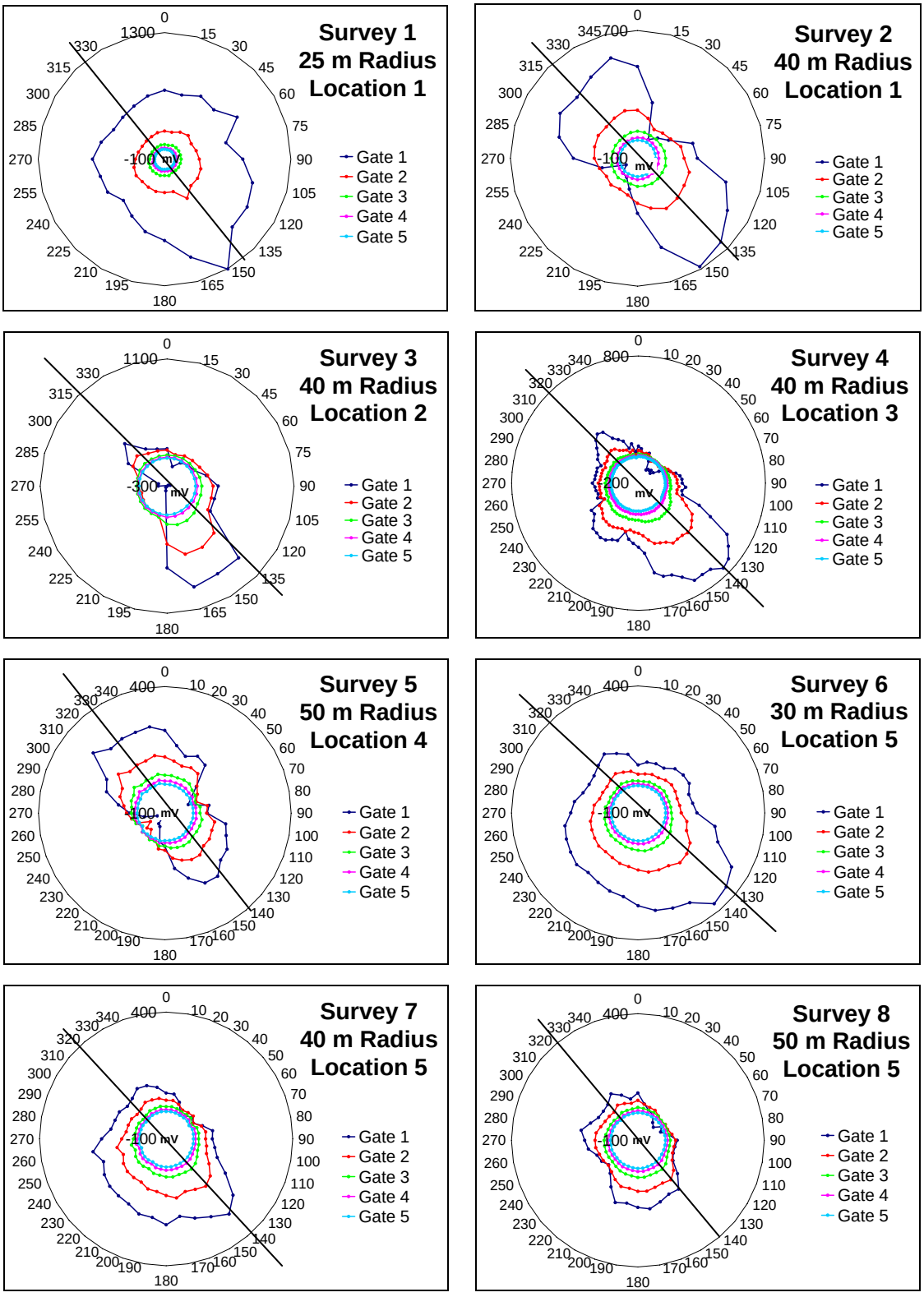

Figure 23. Maximum principal axis orientation for the 8 TDEM surveys. Plots show the voltage [mV] raised in the RX at azimuths from north (φ = 0). Lines indicate the approximate orientation of the maximum principal axis. Notice the orientations are not identical indicating spatial variability or heterogeneity at the field site. The average orientation of the first time gate is 137º as compared to the measured strike of foliation of 146º.

6). In addition, small-scale systematic fractures may be present at the field site. The scale of each of these factors allows superposition of the various effects in order to produce bulk anisotropy detectable at the scale of the surveys. Determining which of these factors do or do not contribute in this study is difficult. It is possible that all of the factors add together to enhance the bulk anisotropy, or that only one of the factor contributes. Care must be taken at this point to understand that the cause cannot be absolutely pinpointed.

Discussion

Recall that the study site is closely bounded by a fault on the east and the basal Hickory Sandstone contact 100 m to the south creating possible spatial variability at the field site (Figures 4 and 5). In addition to possible lateral geologic variations, extensive deep weathering has affected the Packsaddle Schist during Cambrian time as well as the Holocene and Recent. It is inferred that weathering has produced a weathered layer on the Packsaddle Schist that is assumed to be approximated as isotropic in electrical behavior. The thickness of the isotropic layer varies laterally. The thicker the homogeneous layer, the larger the TX-RX separation distance required to detect current flows in the anisotropic schist beneath the isotropic layer.

Quantitative measures and visual inspection of the polar plots indicate that the surveys with a transmitter-receiver loop separation greater than or equal to 40 m demonstrate an anisotropic response characteristic of electromagnetic induction, whereas the surveys with smaller separations exhibit less conclusive anisotropic behavior. Deeper depths are being interrogated by the greater loop separations; therefore, the cause of

anisotropy is likely not contained within shallow depths. This indicates that the effects of weathering reduce the effects of anisotropy near the surface, substantiating the inferred two layer model of an isotropic layer overlying an anisotropic half-space. In addition, the asymmetry of the plots indicates the presence of spatial variability within the field site.

Fractures within the Packsaddle Schist were observed at the field site and may be on scale small enough to detect in this study. The exact orientation and distribution of these fractures is unknown, and they may or may not be parallel to the direction of foliation, not eliminating them as a cause. Therefore, based on examination of the field site and TDEM data the cause of anisotropy at the study site is likely due to foliation, compositional banding, grain boundary cracks, and/or small-scale systematic fractures. This anisotropy exists below an isotropic layer produced by weathering.

DIRECT CURRENT RESISTIVITY SURVEY

Overview

An azimuthal, direct current, apparent-resistivity survey was conducted at the survey site in order to provide an additional independent data set that might reveal anisotropic behavior. The purpose of this survey is to use a proven method of anisotropy detection to support the unproven TDEM method of detection. Direct current geoelectrical surveys measure the same electric properties of the subsurface as electromagnetic induction. Therefore, proving the occurrence of anisotropy using this method indicates the subsurface possesses the necessary properties to generate anisotropic responses in the TDEM survey.

The azimuthal, offset Wenner electrode configuration was used by arranging six equally spaced electrodes along the same line using Advanced Geosciences, Inc. STING R1 ^{TM} resistivity equipment. For each linear array of electrodes, three measurements were made. The first resistance measurement was made with the left four electrodes, the second with the inner four electrodes, and the third with the right four electrodes. The linear array was moved progressively in 10^{o} increments for 180^{o} about a point fixed between the two innermost electrodes. In the Wenner configuration, the two outside electrodes introduce a current into the ground, and the two inside electrodes measure the potential difference between them caused by the DC current. The potential difference is a measure of the electrical resistance between the two inside electrodes, which is a function of the electrode configuration and the electrical attributes of the ground [*Bhattacharya and Patra*, 1968]. This potential difference is expressed as electrical resistivity in ohm meters, which is the inverse of electrical conductivity. The technique

allows geoelectric mapping of the subsurface which gives an idea of the lateral variation of resistance values within a certain depth [*Bhattacharya and Patra*, 1968]. Rotating the linear array of electrodes allows the detection of possible directional variations of electrical resistance which could reflect an anisotropic response. As noted earlier, *Busby* [2000] proposed four measures when assessing the existence of electrical anisotropy. These quantitative measures were used in the analysis of the electromagnetic induction data and will be used again here to assess the anisotropic behavior of the subsurface and aid in determining the cause of anisotropy.

Theory of Electrical Anisotropy

Anisotropy and its effects on electrical resistivity are based on both microstructural and macrostructural features of the subsurface. The direct current resistivity method measures the distribution of potential due to a point source of current. The flow of current relies on the principle of conservation of charge expressed by:

$$div\vec{J} = -\frac{\partial \boldsymbol{q}}{\partial \boldsymbol{t}} \tag{9}$$

where $\vec{J}$ is the current density (A/m^2) and **q** is the charge density (C/m^3) [*Bhattacharya and Patra*, 1968]. Ohm's law relates the current density $\vec{J}$ to the electric field intensity $\vec{E}$ (V/m) in an isotropic medium with the equation:

$$\vec{J} = \frac{1}{\rho}\vec{E} = -\frac{1}{\rho} gradV \tag{10}$$

where ρ is the resistivity (Ωm) and V is the electric potential (volts) [*Bhattacharya and Patra*, 1968]. In an anisotropic medium, the current density $\vec{J}$ requires modification of Ohms's Law as follows:

$$\begin{aligned} J_x &= \sigma_{xx}E_x + \sigma_{xy}E_y + \sigma_{xz}E_z \\ J_y &= \sigma_{yx}E_x + \sigma_{yy}E_y + \sigma_{yz}E_z \\ J_z &= \sigma_{zx}E_x + \sigma_{zy}E_y + \sigma_{zz}E_z \end{aligned} \tag{11}$$

where the electric field in the direction k is σ_{ik} when a unit current density is in the direction of i [*Bhattacharya and Patra,* 1968]. A symmetric six component tensor represents conductivity in this equation. Further transformation of current flow in an anisotropic medium requires definition of longitudinal resistivity ρ_L which is parallel to foliation, and transverse resistivity ρ_T which is normal to foliation. From these variables, the coefficient of anisotropy λ, and the root mean square resistivity ρ_m are defined as

$$\lambda = \sqrt{\frac{\rho_T}{\rho_L}} \text{ and} \tag{12}$$

$$\rho_m = \sqrt{\rho_T \rho_L} \tag{13}$$

respectively [*Bhattacharya and Patra,* 1968]. Applying Laplace's equation to Ohm's Law and solving for potential V, a two dimensional anisotropic medium can be represented by

$$V = \frac{I\rho_m}{2\pi r\left[1+(\lambda^2-1)\sin^2\varphi\sin^2\alpha\right]^{1/2}} \tag{14}$$

where r is the distance from the line source of current I, φ is the angle of orientation relative to the maximum principal direction, and α is the angle of dip from horizontal [*Bhattacharya and Patra,* 1968]. For vertical beds $\alpha = 90^o$, resulting in an elliptical plot of potential V about a central location with the long axis of the ellipse oriented along the strike of foliation. Apparent resistivity parallel to foliation ρ_L is larger than transverse resistivity ρ_T which is normal to foliation, even though true resistivity is larger parallel to

foliation than normal to foliation. As noted earlier, this is due to the electrical "paradox of anisotropy". *Bhattacharya and Patra* [1968] explain the paradox by the fact that since ρ_L is less than ρ_T, current density is greater along the plane of foliation than normal to the plane.

As mentioned earlier, four measures are necessary to analyze azimuthal resistivity data [*Busby*, 2000]. First, a quantitative measure of homogeneity is determined using the two homogeneity index equations below

$$\frac{\sigma\left(\rho_{D1,D2}\right)}{\sigma\left(\left|\rho_{D1}-\rho_{D2}\right|\right)} \quad \text{and} \tag{15}$$

$$\frac{\sigma\left(\rho_{D1,D2}\right)}{\sqrt{meanvalue\left[\left(\rho_{D1}-\rho_{D2}\right)^2\right]}} \tag{16}$$

where ρ_{D1} is the first measurement in the Wenner offset , ρ_{D2} is the second, $\rho_{D1,D2}$ is the average of the first and the second, and σ is standard deviation [*Busby*, 2000]. Data must have a homogeneity index above 1 to be considered sufficiently homogeneous to consider variations to reflect anisotropy and not heterogeneities [*Busby*, 2000]. The second factor determines if azimuthal variations indicate anisotropy. This measure allows discrimination in the data between an elliptical azimuthal response model indicative of anisotropy or a circular azimuthal model indicative of isotropy. R^2 is the percentage of variance, σ^2, from the circular model, which has been removed by the elliptical model and is expressed with the equation

$$R^2 = \frac{\left(\sigma^2_{(circle)} - \sigma^2_{(ellipse)}\right)}{\sigma^2_{(ellipse)}} \tag{17}$$

[*Busby*, 2000]. A perfectly anisotropic model has an R^2 value of 1, where low values

around 0.2 indicate an isotropic model. Quantitative measures of anisotropy include percentage variation about the average and the coefficient of anisotropy, which are, respectively

$$\pm 0.5\left[\frac{\left(\rho_{\max}-\rho_{\min}\right)}{\rho_{average}}\right]100\% \text{ and} \tag{18}$$

$$\lambda=\sqrt{\frac{\rho_T}{\rho_L}}\,. \tag{19}$$

This third method of measurement of anisotropy is also used to describe the orientation of the ellipse by determining the strike azimuth of the major axis of the ellipse. According the fourth and final factor in interpreting and analyzing azimuthal resistivity data is determining the underlying cause of anisotropy. A number of causes of anisotropy are mentioned such as sub-vertical fractures, aligned thin beds, and schistosity. This method allows interpretation of anisotropy which would have previously been discounted; however, data can be noisy and care must be taken when determining the cause

STING R1™ Results

An azimuthal Wenner offset resistivity survey was conducted at Location 3 in the survey area (Figure 9). Combined, the two outside measurements of the survey represent outer resistance values 360º around the center of rotation. The inside measurements represent inner resistance values 180º around the center of rotation and are mirrored to indicate 360º representation. Figure 24 is a polar plot of the apparent resistivity readings for the outer and inner measurements, ρ_{D1} and ρ_{D2}, respectively, and the average of the two measurements $\rho_{D1,D2}$, where zero azimuth is north. The average $\rho_{D1,D2}$ minimizes the effects of dip and lateral effects which exhibit 360º symmetry, allowing the 180º The

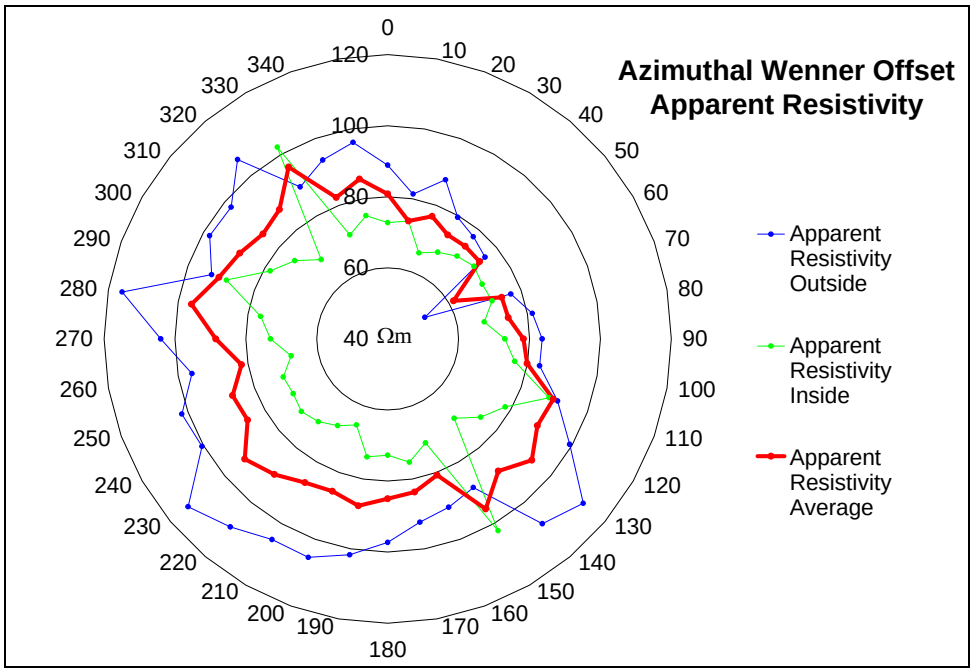

Figure 24. Direct current apparent resistivity data, Location 3. Data are plotted on a polar chart where azimuth 0º corresponds to north and the values are apparent resistivity in Ωm. This plot can be visualized as a plan view map of apparent resistivity at Location 3 with the strike of foliation trending 146º. Apparent resistivity outside (blue) is the measurement taken with the outside four electrodes at a given azimuth, and apparent resistivity inside (green) is the measurement taken with the inside four electrodes. Apparent resistivity average is the average of the inside and outside measurements for a given azimuth. The average reduces the spatial variability within the data.

azimuthal symmetry of anisotropy to be differentiated [*Watson and Barker*, 1999]. shape of the polar plot is elliptical and matches the theoretical ellipse of an anisotropic medium based on Equation 14 (Figure 25).

1 *Is the subsurface sufficiently homogeneous to detect anisotropy*?

Interpretation of an anisotropic medium using azimuthal surveying techniques includes determining if the medium is sufficiently homogeneous to determine if anisotropy is present. *Busby* [2000] defined a homogeneity index with two equations (15 and 16). For the survey data these values are 1.57 and 0.39, respectively. These values determine if the anisotropy measure exceeds the measure of dispersion caused by inhomogeneity using standard deviation and mean deviation respectively. The first value is well above one, indicating that anisotropic homogeneous effects are well above effects influenced by inhomogeneity. The second value 0.39 is a more stringent test of dispersion and reveals the opposite. The first value has been accepted as the best indicator by empirical studies [*Busby*, 2000]. Therefore, by these methods, the survey data can be said to be sufficiently homogeneous to determine variations due to anisotropy.

2 Are the azimuthal variations significant enough to indicate anisotropy?

The statistic R^2 for this data is 0.77 or 77%. This represents the goodness-of-fit to an elliptical model (Equation 17). A value of 1.0 (100%) corresponds to a perfect ellipse; whereas low values around 0.2 (20%) indicate isotropic behavior. The value for this data indicates it sufficiently fits the elliptical model indicating anisotropy.

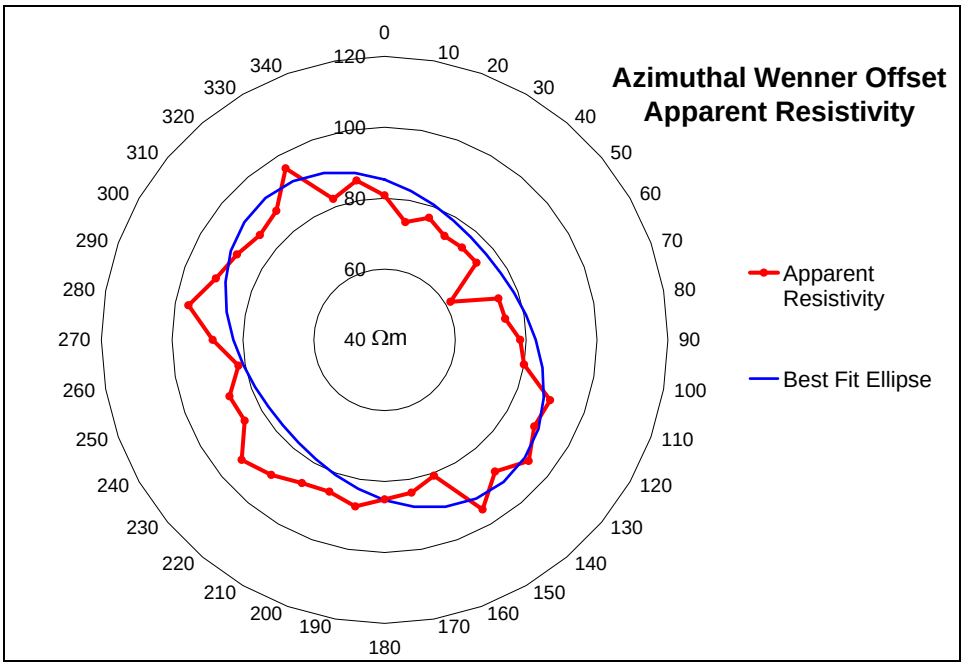

Figure 25. Direct current apparent resistivity best-fit ellipse. Apparent resistivity is indicated in red and the best-fit ellipse for this data (Equation 14) is indicated in blue. Notice that the orientation of the maximum principal axis of the best-fit ellipse is oriented 149º as compared to the direction of the measured strike of foliation of 146º.

3 Can the anisotropy be described quantitatively?

Quantitatively, the orientation of the best fitting ellipse and parameters quantifying anisotropy are sufficient to describe the anisotropy (Table 3) [*Busby*, 2000]. The orientation of the best fit ellipse is 149º and the parameters of anisotropy are 34% and 1.57, respectively (Equations 18 and 19). Recall that the orientation of the TDEM contour is 137º, and measured strike of foliation is 146º. Overall, the quantitative analysis indicates that these data can be confidently used to interpret the anisotropic signature of the subsurface.

4 What is the cause of anisotropy?

The electrical response in a direct current resistivity survey is caused by the same transport properties affecting the response of time-domain electromagnetic surveys. Therefore, the possible causes discussed previously include mineral foliation, mineral lamination, compositional banding, grain boundary cracks, weathering, and small-scale systematic fracture systems.

In summary, this additional independent resistivity survey exhibits apparent resistivity in the form of an ellipse with the major axis (direction of maximum conductivity) oriented 149º, which is nearly parallel to schist foliation of 146º and the TDEM data of 137º. Further analysis of data indicates the apparent electrical conductivity parallel and perpendicular to foliation are 0.0163 S/m and 0.0094 S/m, respectively. Results closely match the TDEM data in both orientation and electrical conductivity values.

Table 3. Quantitative measures of the direct current resistivity data. ρ_{D1} is the apparent resistivity measured with the inside four electrodes in the Wenner configuration, ρ_{D2} is the apparent resistivity measured with the outside four electrodes, and $\rho_{D1,D2}$ is the average of ρ_{D1} and ρ_{D2}. R^2 is the reduction in variance and λ is the coefficient of anisotropy found by the ratio of the maximum and minimum principal axes.

	R^2	Axis Strike [degrees]	λ	Percent Anisotropy	Average Value [Ωm]
ρ_{D1}		148°	1.49	± 34%	93.72
ρ_{D2}		150°	1.25	± 25%	74.49
$\rho_{D1,D2}$	77%	149°	1.25	± 21%	84.00

SEISMIC SURVEY

Overview

An azimuthal seismic survey was conducted at Location 5 with 36 geophones arranged in a circle. The purpose of this survey is to determine if P-wave velocity, V_P, is dependent on azimuth, aiding the discussion of the cause of anisotropy. Observed P-wave velocities in previous studies are greater along strike than across strike of anisotropy [*Song et al*., 2004; *Godfrey et al.*, 2000]. The 36 geophones were arranged in a circle of radius 17.2 m with 10º separations. Source shots were arranged in a concentric circle of radius 30 m (Figure 26). An additional shot was collected at the center of the circle. A 10 pound sledge striking a metal plate was used as the source and stacked five times at each shot location. A Geometrics Strata View^{TM} 36 channel seismograph was used for the survey. An example seismograph from a source shot located due south of the center is shown in Figure 27.

Travel times for the first P-wave arrivals were recorded for the center shot. In addition, travel time to the geophone farthest (47.19 m) from each of the 36 concentric shots were recorded and collectively shown on a polar plot according to the position of the geophone. Zero degrees azimuth corresponds to north on the polar plots. A best-fit contour was found for the plots, and used to quantitatively interpret the data.

Seismic Theory

In seismic methods, waves travel at the surface (surface waves) and within the subsurface (body waves). Body waves are compressional P-waves and shearing S-waves.

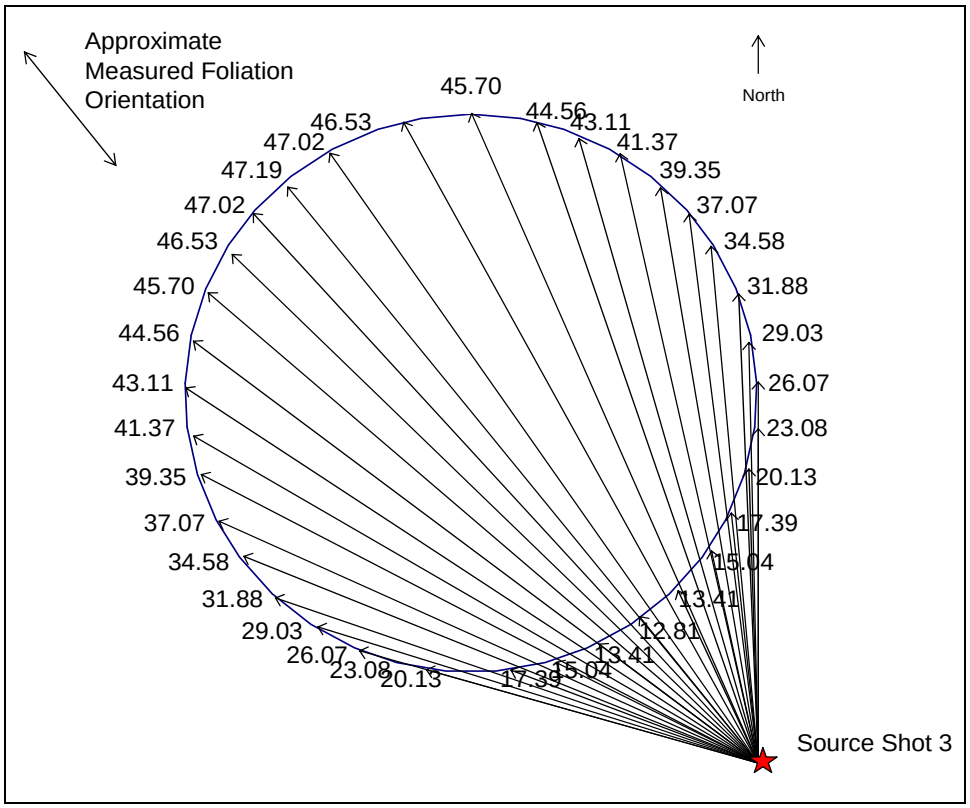

Figure 26. Seismic survey orientation. This is an example of the orientation of the seismic survey with source shot 3 located at the same azimuth as geophone 3, which is 30º from south moving counterclockwise. Arrows indicate the P-wave path from the source to receiver. Values indicate the distance in meters of this path. The source is located 30 m from the center of the circle. The shortest path (12.8 m) is to geophone 3, and the farthest path is to geophone 21 (47.2 m). Note the orientation of measured foliation compared to the paths traveled by the compressional waves.

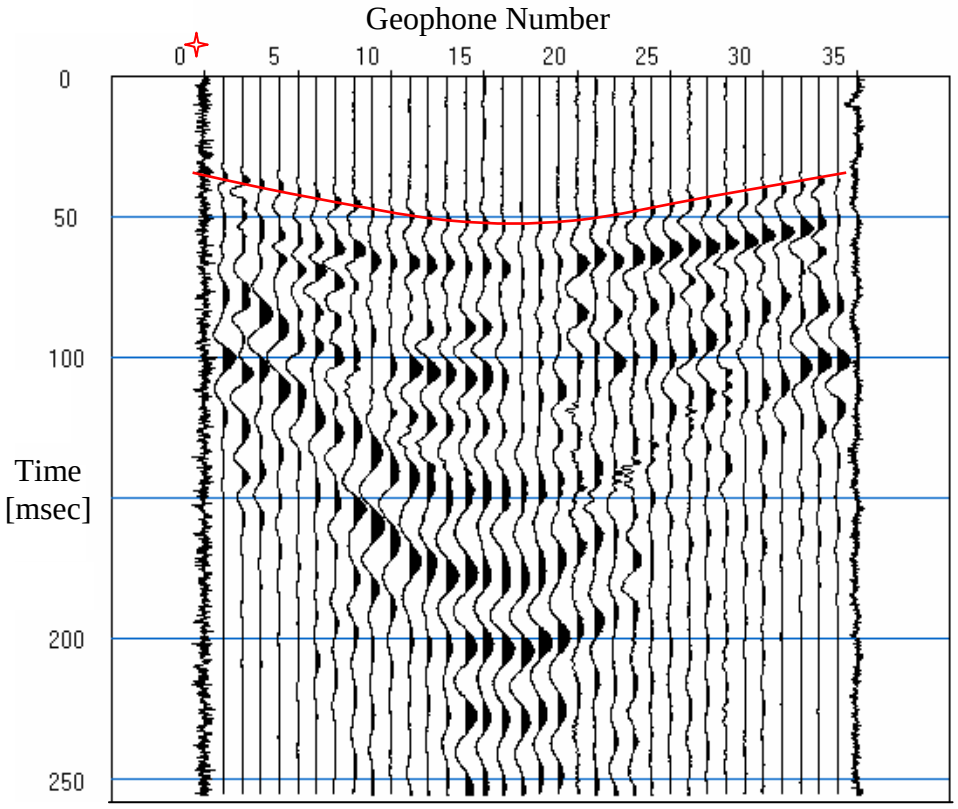

Figure 27. Shot 1 seismograph. Approximate first P-wave arrival is indicated by the red line. Travel time in milliseconds increases downward. The numbers at the top of the graph indicate the geophone numbers from 1 to 36 which are arranged in a circle rotating counterclockwise starting at south. The red star indicates that the source shot is located on a concentric circle as the geophones at the same azimuth as geophone 1, 30 m from the center. Geophone 18 indicates the location farthest from the shot, as evident by the largest travel time.

P-waves compress and dilate particles in the direction of propagation. P-waves travel the fastest, and therefore are the first to arrive. S-waves entail shearing motions transverse to the direction of propagation. This study will focus on the behavior of P-waves. The general relationships between P-waves, elastic moduli, and density of a material are expressed by the equation

$$V_P = \sqrt{\left(\frac{K + 4\mu/3}{\rho} \right)} \tag{20}$$

where ρ is density, K is the bulk modulus, and μ is the shear modulus. The two types of surface waves are Rayleigh waves and Love waves. Rayleigh waves travel along the ground surface in a retrograde elliptical motion along the plane of travel [*Sharma,* 1997]. These waves are usually termed 'ground roll' and travel about 0.9 V_s. Love waves only travel across a surface if it is not uniform.

Subsurface contrasts in acoustic impedance cause compressional waves to reflect, refract, or diffract at the boundary. Acoustic impedance is the product of the density of the medium and P-wave velocity in the medium. In refraction methods, seismic waves travel mainly horizontal along an interface. This happens when the incident wave strikes the interface at a critical angle causing the wave to refract along the interface. The travel times of refracted waves depend on the time it takes to reach the interface, the time traveling along the interface, and the time to return to the receiver. Equation 21 represents the travel time for a refracted wave in a simple two layer medium

$$T = \frac{2h_1}{V_1 \cos i_c} + \frac{x - 2h_1 \tan i_c}{V_2} \tag{21}$$

with P-wave velocities V_1 and V_2 separated by depth h_1. The majority of the distance traveled by a refracted wave is along the interface, which is faster than the first layer. For this reason, refracted waves are the first to arrive if the receivers are sufficiently far from the source relative to the depth of the layer interface.

Factors Affecting Velocity

From the P-wave velocity (Equation 20), it is apparent that velocity is dependent on the density and elastic properties of the medium. First look would indicate that as density increases, the velocity decreases; however, the opposite is true because the bulk modulus and shear modulus also depend on density and increase more rapidly than density alone. Factors that affect density affect velocity. Some factors include porosity, pore fluids, pore shape, fracturing, and composition of the rock matrix [*Sharma*, 1997]. Porosity affects density because the fluids that occupy the space have different elastic properties; the content of these fluids such as air or water can dramatically slow velocities.

In metamorphic rocks, velocities may be 10-20% higher parallel to foliations than perpendicular to foliations [*Sharma*, 1997]. The variation in velocity is due to elastic anisotropy within the subsurface. Sources could include bedding planes, regular joints, foliation, oriented microcracks and textures, and anisotropy of stress [*Song et al.*, 2004]. Metamorphic rocks exhibit transverse anisotropy, where elastic properties are equal along strike of the foliation and different across the strike of foliation [*Song et al.*, 2004]. Preferred orientation of minerals, compositional layering, parallel discontinuities

or some combination of these microstructures (Figure 6) form approximately planar structures encompassed within the term foliation [*Song et al.*, 2004].

Seismic Results

This study uses the seismic refraction method to compare the velocities as a function of measurement direction. Plots of travel time for the first P-wave arrivals are shown for the center shot (Figure 28) and for the geophones farthest from each shot (Figure 29). A best-fit contour is found for the center shot plot using the equation

$$T = \sqrt{\left(T_{\max}\cos(\varphi)\right)^2 + \left(T_{\min}\sin(\varphi)\right)^2} \tag{22}$$

where T_{max} is the largest travel time, T_{min} is the minimum travel time, and φ is the azimuth of the geophone location with respect to the strike of foliation. According to Equation 21, the higher travel time value indicates a slower velocity refracted off the same interface. Therefore, the maximum principal axis of the ellipse corresponds to the slowest velocity, and the minimum principal axis corresponds to the fastest velocity. Orientation of the minimum principal axis of the best-fit contour is 140º, which correlates closely to the orientation of the measured foliation of 146º.

Plots of travel times for the center shot closely match the best fitting contour with the exception of the southwest quadrant. The homogeneity index is 2.06 for this data, indicating the variations due to anisotropy are greater than the variations due to lateral effects. This allows further quantitative measurements to be made to determine the degree of anisotropy detected. The coefficient of anisotropy for the best fitting contour is 1.24. This value is found by dividing the maximum principal axis of the best fitting contour by the minimum principal axis. Percent anisotropy for the contour is 22%. This

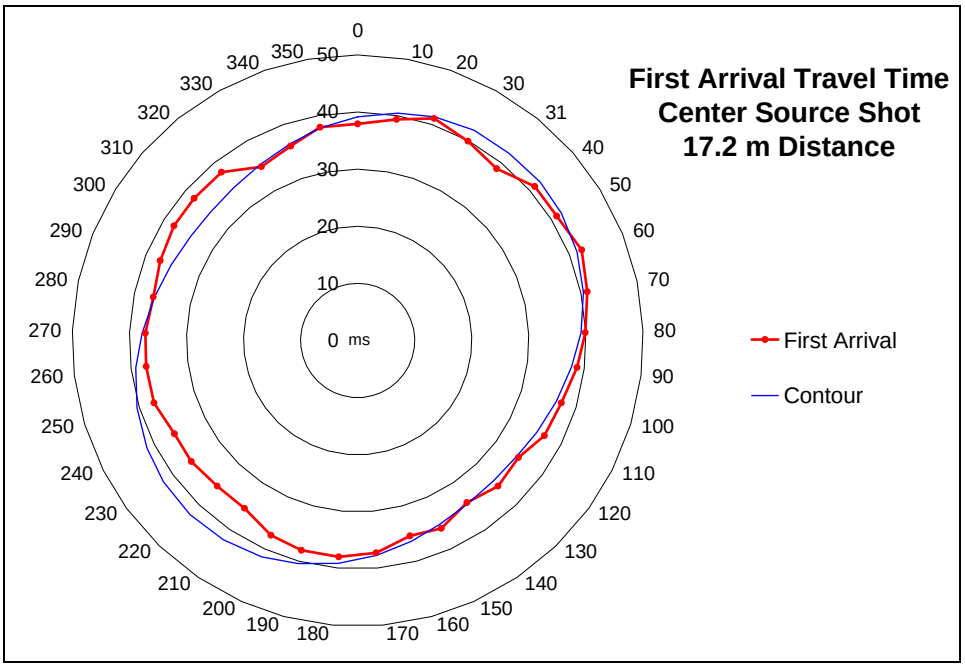

Figure 28. Seismic first arrival travel time for the center source shot. The red line is the first arrival travel time recorded at geophones located at given azimuths from north (φ=0). The blue line represents the best-fit contour manually adjusted to fit the data (Equation 22). The maximum principal axis of the contour is oriented 50º, indicating the direction of slowest seismic velocity (Equation 21). The minor axis of the contour is oriented 140º, as compared to the measured strike direction of foliation of 146º.

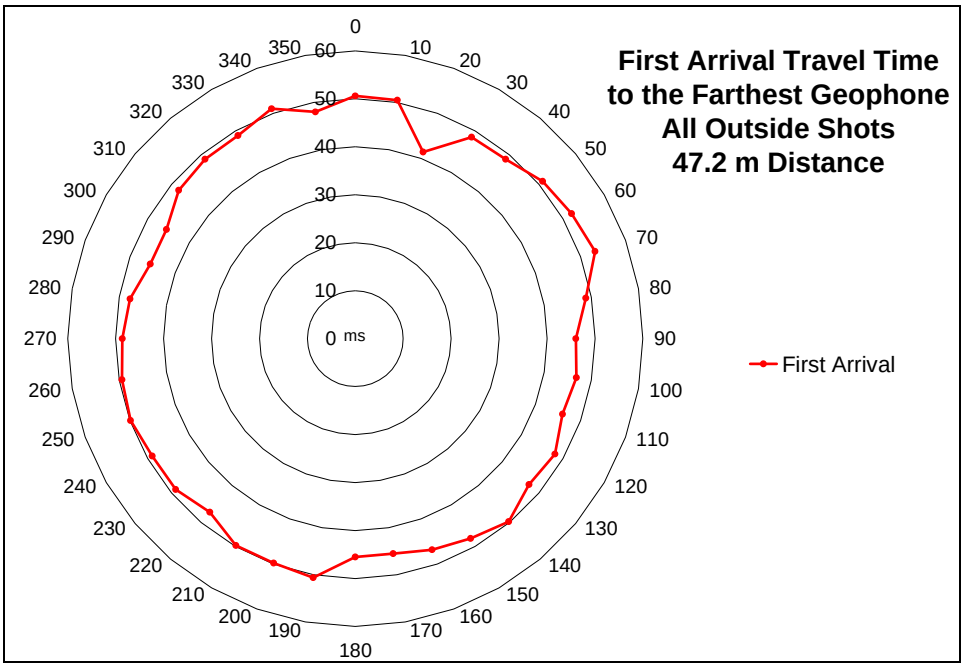

Figure 29. Seismic first arrival travel time for all outside source shots. The circular shape of the data suggests no directional variations.

value is the difference between the maximum and minimum principal axes of the best fitting contour divided by the average of the two. Travel times from all seismographs demonstrate a homogeneity index of 0.87. An index value below 1.0 signifies the variations due to inhomogeneities are greater than the variations due to anisotropy, preventing further quantitative analysis of the data. Further research is necessary to determine the discrepancies in this data as compared to the data of the center shot.

Discussion

A measure of ultrasonic velocity (~160 kHz) measurements on amphibole and biotite schist core samples by *Song el al.* [2004] were conducted at varying confining pressures. Velocity increased with confining pressure, suggesting the closure of microcracks, but the foliation-induced anisotropy was relatively unaffected. However, the anisotropy does not decrease with pressure in both amphibole schist and biotite schist, indicating that the closing of fractures does not affect anisotropy, minimizing microcracks as a cause of anisotropy and emphasizing foliation as the primary parameter inducing anisotropy in intact foliated metamorphic rock.

Recent/Holocene and Cambrian-age weathering may have increased random microcracks oblique to foliation, therefore dramatically decreasing the velocity and decreasing the effects of anisotropy. Anisotropy was detected according to the first arrival times in the center shot seismograph, implying that we are “seeing” below the Holocent/Recent weathered zone. Percent anisotropy for this data is 22% compared to the findings of *Godfrey et al.* [2000] of 9-20% anisotropy in schists.

Due to the low confining pressure and effects of weathering, grain boundary cracks, or microcracks, associated with the cleavage planes of foliation are believed to produce an anisotropic elastic signature at the field site. This property causes a slower velocity across the cracks than along the cracks. In addition, alignment of minerals due to foliation and lamination [*Song et al.*, 2004], and compositional layering [*Melia and Carlson*, 1984] have been shown to exhibit elastic properties under all pressure conditions in foliated rocks, leading to the inclusion of these factors as contributing to elastic anisotropy at the field site. Two principal directions are evident in the center shot travel time ellipses, indicating that elastic anisotropy at the field site exhibits one mirror plane of symmetry. This indicates that the contribution of systematic fracture systems is either parallel to metamorphic foliation, or a minor component not apparent in the data.

Therefore, by application of previous seismic studies of elastic anisotropy, this seismic survey has determined possible causes of elastic anisotropy at the field site to include microcracks, foliation, compositional layering, and possibly systematic fracture systems. Weathering affects anisotropy by producing microcracks that are randomly oriented, reducing the anisotropic signature. The orientation of the detected elastic anisotropy correlates to the orientation of electrical anisotropy detected by both TDEM and direct current resistivity methods.

FORWARD MODELING

Overview

This section of the study is a continuation of the research set forth by the theory in the paper by al-Garni and Everett (2003). Their research numerically modeled the response of a frequency domain, controlled source, electromagnetic system deployed over an anisotropic half-space idealized as a configuration of vertical aligned fractures (Figure 1). Calculations for the model can be seen in Appendix A. The response varied depending on the orientation of the transmitter and receiver with respect to the across-strike conductivity $\sigma_{\perp}$ and along-strike conductivity $\sigma_{||}$. According to the results, apparent conductivity is larger when the transmitter and receiver are oriented across-strike ($\varphi=0^{o}$), than when they are oriented along-strike ($\varphi=90^{o}$), indicating that the across-strike conductivity $\sigma_{\perp}$ is larger than the along-strike conductivity $\sigma_{||}$ (Figure 2). The reverse is actually true, and application of a paradox of anisotropy is applied (Figure 13) [*al-Garni and Everett*, 2003].

For this study, a trial-and-error method using different along- and across-strike electrical conductivities will be used to compute multiple models. Comparison between the theoretically calculated models and the data collected at the field site will allow approximate electrical conductivity values to be determined. To begin research, the formulas were re-cast in the time-domain. A computer code adapted these formulas by using 30 different frequency-domain responses to resemble a broadband time-domain response. Parameters in the model include the transmitter loop current set at 3.0 amps and the transmitter loop radius set at 5.0 m. Variables in the model include across-strike

conductivity, $\sigma_{\perp}$, along-strike conductivity, $\sigma_{||}$, and azimuth. Azimuth was varied by 10 degrees from 0º to 90º for each set of $\sigma_{\perp}$ and $\sigma_{||}$. Due to the symmetry of the data, results from 0º to 90º can be mirrored to complete a 360º model similar to the field survey. In this text we will use the term model to indicate the collection of data from the 360º response calculated for a set value of $\sigma_{\perp}$ and $\sigma_{||}$. Varying conductivities in different models allows a match between the numerical computations and the TDEM field data to be found and hence determines $\sigma_{\perp}$ and $\sigma_{||}$ at the field site. In addition, multiple models provided a better understanding of how different conductivities control the electromagnetic response of an electrically anisotropic medium.

Forward Modeling Results

Results from the derivation of the time-domain electromagnetic response over a transverse anisotropic half-space are shown in Figures 30 and 31. Polar plots indicate a two-lobed signature similar the TDEM data. Azimuths $\varphi = 0º$ and $\varphi = 180º$ and correlate with the along-strike direction. Similarly, azimuths $\varphi = 90º$ and $\varphi = 270º$ and correlate with the across-strike direction. Plots are oriented with the maximum principal axis at 150º to correspond to the measured foliation direction, and are representative of a 10º sampling. Varying conductivities along and across strike alter the voltages by azimuth (Figures 30 and 31, respectively). Higher along strike conductivity “stretches” the maximum principal axis value. Larger differences between along and across strike conductivities result in a “pinch in” of the across-strike voltage value. The best fit model

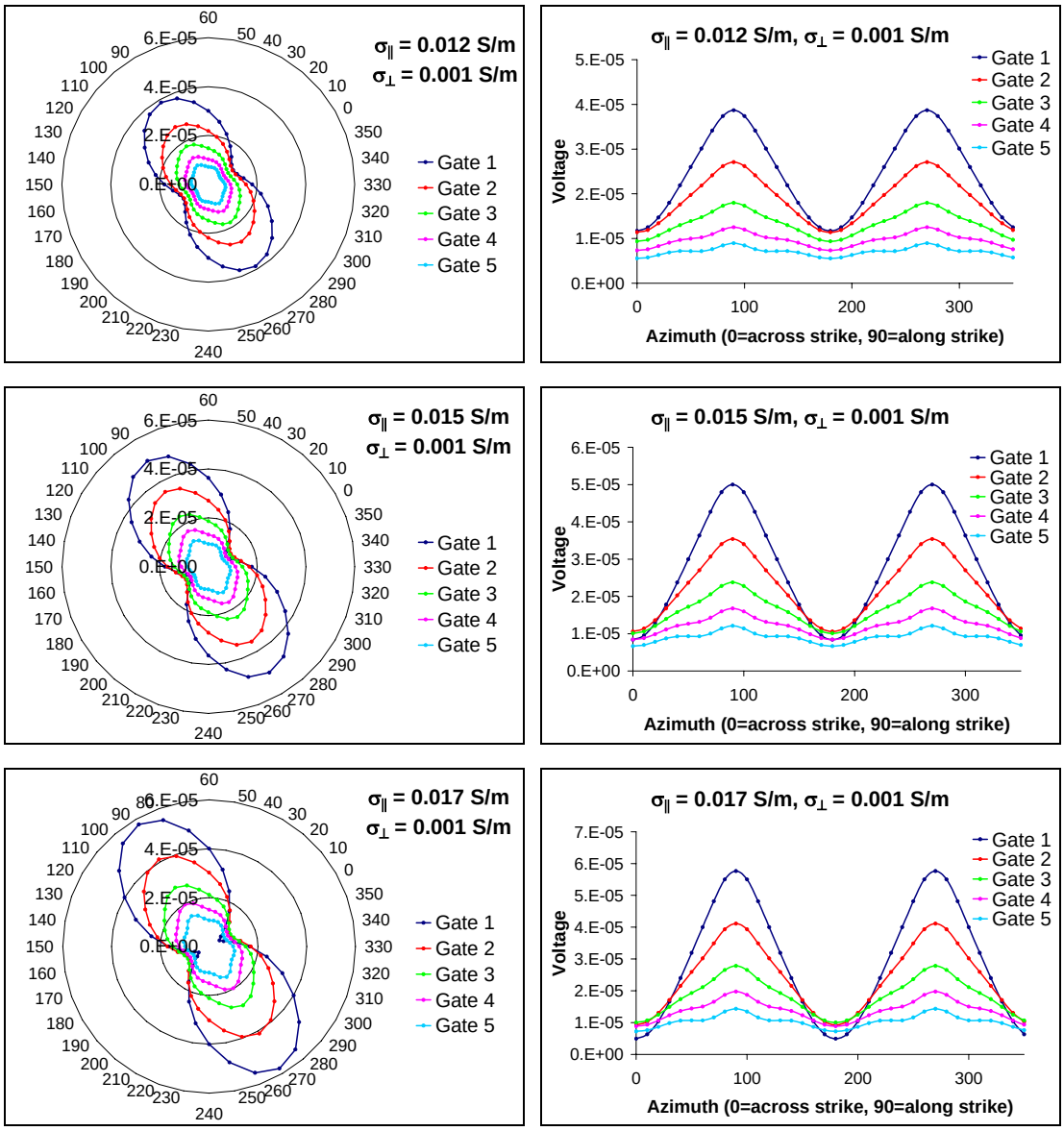

Figure 30. Numerical model responses with varied along-strike conductivity. Polar plots of the calculated response are indicated on the left with across strike conductivity $\sigma_{\perp}$ (φ=0) remaining constant at 0.001 S/m (Siemens per meter), and along strike conductivity $\sigma_{||}$ (φ=90) increasing from 0.012 to 0.017 S/m. The plots are oriented so that the along-strike direction (φ=90) is approximately parallel to the strike of foliation of 146º. Higher along strike conductivity $\sigma_{||}$ increases the response in the along strike direction (φ=90) and causes the response to "pinch in" more in the across strike direction (φ=0). Plots on the right indicate the same data displayed as a function of azimuth where the peaks indicate the along strike direction and the troughs indicate the across strike direction.

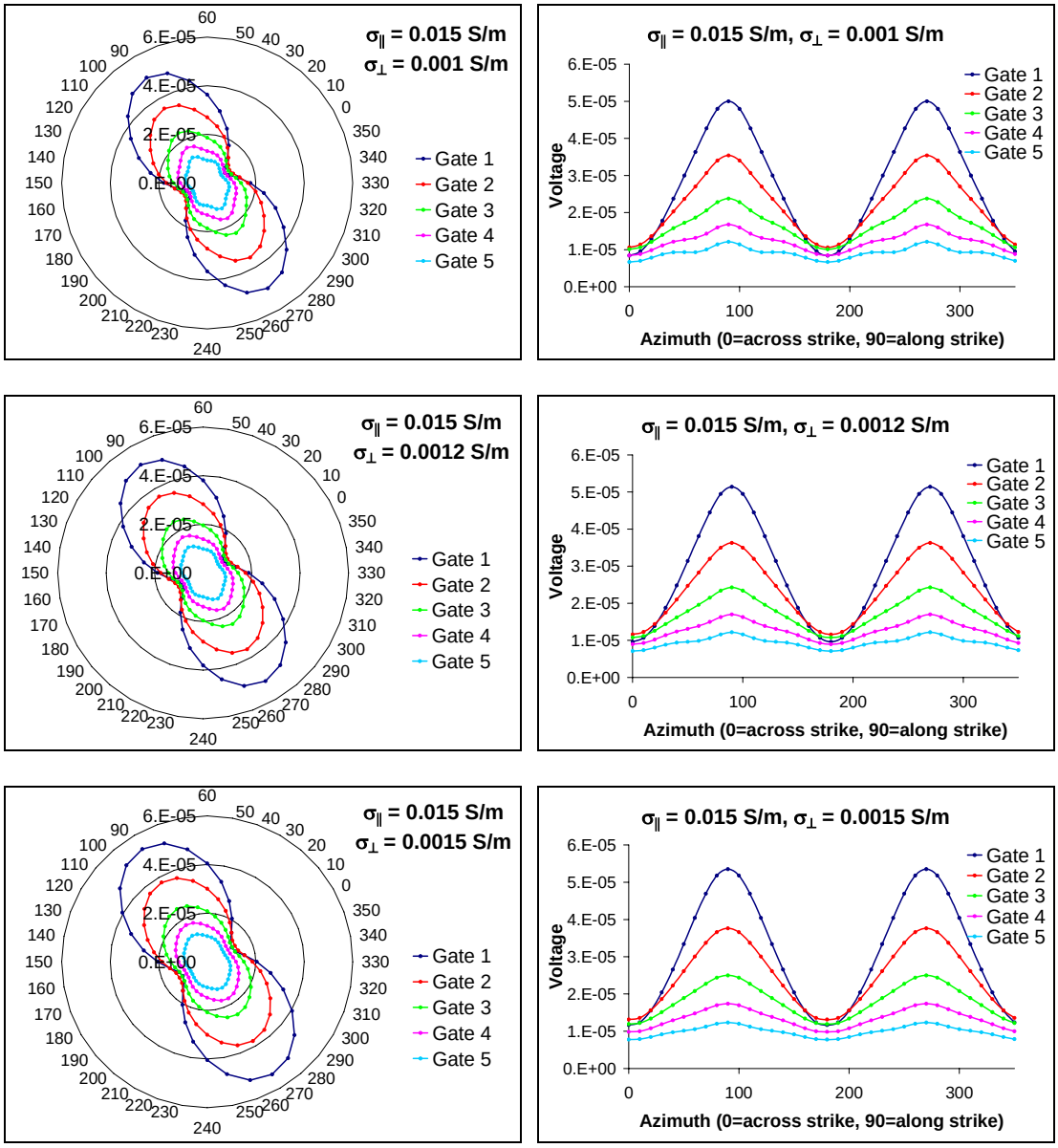

Figure 31. Numerical model responses with varied across-strike conductivity. Polar plots of the calculated response are indicated on the left with along strike conductivity $\sigma_{\|}$ (φ=90) remaining constant at 0.015 S/m (Siemens per meter), and across strike conductivity $\sigma_{\perp}$ (φ=0) increasing from 0.001 to 0.0015 S/m. The plots are oriented so that the along-strike direction (φ=90) is approximately parallel to the strike of foliation of 146º. Higher across strike conductivity causes the lobes to widen and decreases the "pinch in" in the across strike direction. Plots on the right indicate the same data displayed as a function of azimuth where the peaks indicate the along strike direction and the troughs indicate the across strike direction.

to the TDEM data based on R^2 and λ values indicates the subsurface conductivity along strike is approximately 0.015 S/m and across strike is 0.0012 S/m (Figure 32, Table 4). This correlates well with the expected range of mica schist conductivity between 0.05 and 0.0001 S/m, and the DC along- and across-strike conductivities of 0.0163 S/m and 0.0094 S/m, respectively [*McNeill*, 1980]. At later time, the modeled voltages appear less anisotropic because at late time the receiver is measuring a voltage generated by an average across- and along-strike secondary magnetic field response representative of deeper currents. Late time responses also break down in the computer code producing "wiggles" in the plots. Further studies are necessary to eliminate the source of this deviation at late time.

Early-time matching of the numerical model with TDEM data confirms the detection of anisotropy and allows determination of the electrical conductivity values within the subsurface. Deviation from the theoretical response of the data also provides an insight into other possible geological factors affecting conductivity within the subsurface, aiding in the interpretation process.

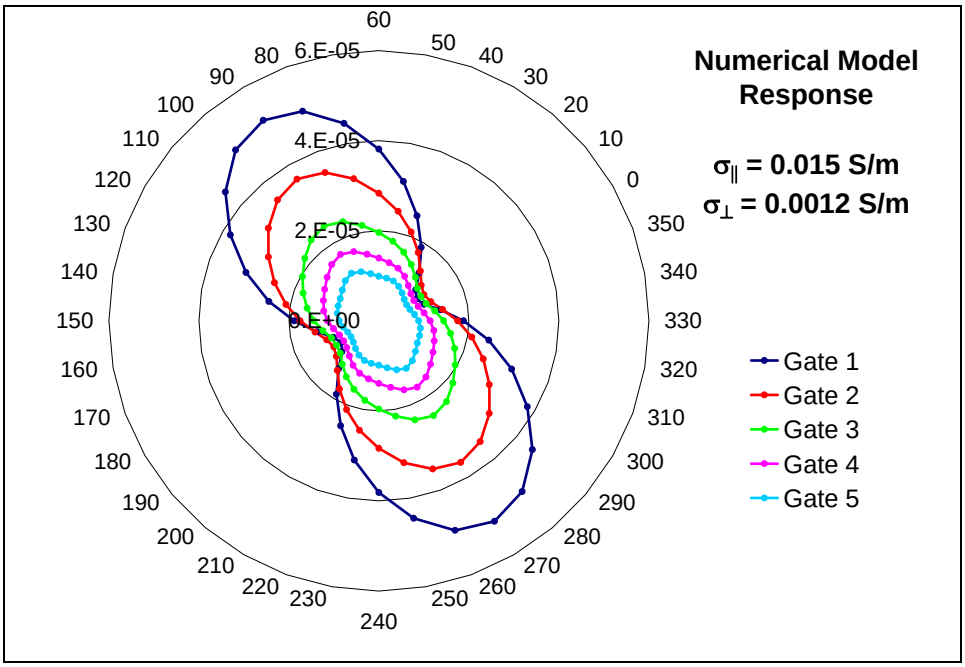

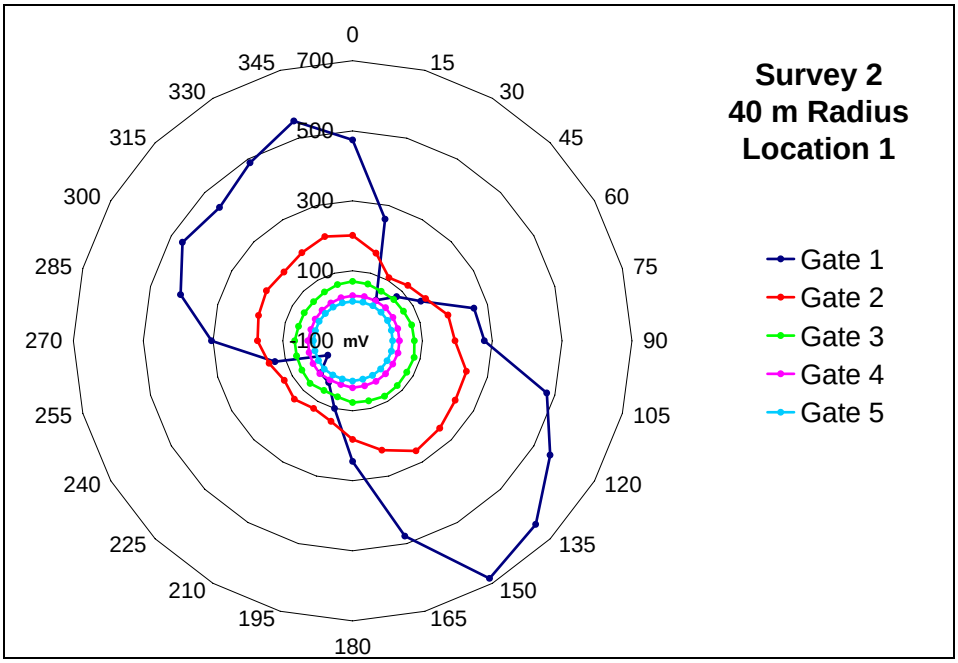

Figure 32. Comparison of numerical model response with Survey 2 data. The numerical response is oriented in the same along strike direction as Survey 2. Both plots have a two-lobed contour and similar coefficients of anisotropy and percent anisotropy (Table 4), making this model a good fit for the data which narrows the along strike and across strike electrical conductivities at the field site.

Table 4. Quantitative measures of the numerical models. Survey 2 measures are included for comparison. The conductivities for each model are indicated along with the maximum, minimum, and average values in volts. λ is the ratio of the maximum and minimum responses.

$\sigma_{//}$ [S/m]	$\sigma_{\perp}$ [S/m]	Gate	Max [V]	Min [V]	Average [V]	Percent Anisotropy	λ
Survey 2		1	6.84E+02	-1.80E+01	3.13E+02	81%	6.16
		2	2.63E+02	1.08E+02	1.79E+02	36%	1.56
		3	8.27E+01	5.77E+01	6.98E+01	3%	1.20
		4	3.49E+01	2.33E+01	3.04E+01	8%	1.22
		5	1.57E+01	1.01E+01	1.33E+01	11%	1.25
0.008	0.001	1	2.41E-05	1.24E-05	1.81E-05	32%	1.94
		2	1.65E-05	9.94E-06	1.31E-05	25%	1.66
		3	1.07E-05	7.22E-06	8.90E-06	19%	1.48
		4	7.27E-06	5.21E-06	6.20E-06	17%	1.40
		5	5.04E-06	3.72E-06	4.35E-06	15%	1.35
0.01	0.001	1	3.17E-05	1.26E-05	2.17E-05	44%	2.51
		2	2.16E-05	1.10E-05	1.61E-05	33%	1.97
		3	1.42E-05	8.48E-06	1.12E-05	25%	1.67
		4	9.76E-06	6.37E-06	8.00E-06	21%	1.53
		5	6.87E-06	4.67E-06	5.71E-06	19%	1.47
0.012	0.001	1	3.87E-05	1.17E-05	2.45E-05	55%	3.31
		2	2.71E-05	1.14E-05	1.89E-05	42%	2.38
		3	1.80E-05	9.38E-06	1.35E-05	32%	1.91
		4	1.25E-05	7.34E-06	9.77E-06	27%	1.71
		5	8.94E-06	5.55E-06	7.10E-06	24%	1.61
0.015	0.0015	1	5.35E-05	1.16E-05	3.13E-05	67%	4.59
		2	3.76E-05	1.31E-05	2.47E-05	50%	2.86
		3	2.50E-05	1.19E-05	1.82E-05	36%	2.09
		4	1.74E-05	9.85E-06	1.34E-05	28%	1.77
		5	1.23E-05	7.77E-06	9.93E-06	23%	1.59
0.015	0.0012	1	5.14E-05	9.61E-06	2.93E-05	71%	5.35
		2	3.63E-05	1.16E-05	2.33E-05	53%	3.13
		3	2.43E-05	1.08E-05	1.72E-05	39%	2.25
		4	1.70E-05	8.97E-06	1.28E-05	31%	1.90
		5	1.22E-05	7.11E-06	9.47E-06	27%	1.72
0.015	0.001	1	5.00E-05	8.36E-06	2.79E-05	75%	5.98
		2	3.54E-05	1.06E-05	2.23E-05	56%	3.34
		3	2.38E-05	1.01E-05	1.65E-05	41%	2.36
		4	1.68E-05	8.42E-06	1.23E-05	34%	1.99
		5	1.21E-05	6.66E-06	9.15E-06	30%	1.82
0.015	0.0008	1	4.88E-05	7.00E-06	2.66E-05	79%	6.97
		2	3.48E-05	9.51E-06	2.14E-05	59%	3.66
		3	2.36E-05	9.26E-06	1.59E-05	45%	2.54
		4	1.68E-05	7.77E-06	1.19E-05	38%	2.16
		5	1.23E-05	6.13E-06	8.85E-06	35%	2.01
0.017	0.001	1	5.76E-05	4.94E-06	2.95E-05	89%	11.67
		2	4.11E-05	9.30E-06	2.43E-05	66%	4.42
		3	2.78E-05	1.00E-05	1.84E-05	48%	2.77
		4	1.98E-05	8.86E-06	1.39E-05	39%	2.23
		5	1.44E-05	7.24E-06	1.05E-05	34%	1.98

CONCLUSION

Time-domain electromagnetics can detect anisotropy in an approximately homogeneous metamorphic schist with uniform striking and steeply dipping foliations. The geologic model of the study site consists of an isotropic soil layer overlying vertically oriented transverse anisotropic schist. The confidence of anisotropic response relies on the separation distance between the transmitter loop and the receiver loop. The reason for this stipulation lies in the theory of electromagnetic induction. The larger separations allow measurements to probe deeper structures; therefore a larger separation is necessary to detect the anisotropic schist beneath the isotropic layer of a certain thickness. Asymmetry of the TDEM data also indicates the presence of spatial variability within the field site

Direct current resistivity aided in establishing the study site as a geological medium that can be represented as an anisotropic half-space by exhibiting a close match in orientation and conductivity values to the TDEM data. Seismic refraction data also indicated an anisotropic response, but was less conclusive. Interpretation of the TDEM data altered this simple model to include an overlying isotropic layer and indicated spatial variability at the field site. Results from the TDEM survey were more definitive than those of the resistivity and seismic surveys. In addition, TDEM surveying was less invasive and most rapidly and easily collected than both the resistivity and seismic methods, making this a promising method for anisotropy detection.

The Packsaddle schist is a metamorphic rock exhibiting foliations that create a vertically transverse anisotropy that can be detected based on the elastic and transport

properties of the rock. The cause of anisotropy cannot be pinpointed to one source, but is an accumulation of the effects of foliation, compositional banding, grain boundary cracks, and systematic fracture systems that add together to produce bulk anisotropy that is detectable on the scale of the surveys in this study.

The forward modeling conducted based on previous frequency domain electromagnetic research sufficiently modeled the data collected over an anisotropic half-space. Re-casting the equations in the time-domain allowed the conductivities across- and along- the strike of foliation to be determined as 0.015 S/m and 0.0012 S/m, respectively, which correlate closely with values expected of metamorphic rocks. Agreement between the theoretical simulations of an electromagnetic response with actual field data provides a robust detection of anisotropy.

REFERENCES

Al-Garni, M. and M. E. Everett, The paradox of anisotropy in electromagnetic loop-loop responses over a uniaxial half-space, *Geophysics, 68*, 892-899, 2003.

Bhattacharya, P.K., and H.P. Patra, *Direct current geoelectric sounding*: *Methods in geochemistry and geophysics*, Elsevier Publishing Company, Amsterdam, Netherlands, 1968.

Busby, J.P., The effectiveness of azimuthal apparent-resistivity measurements as a method for determining fracture strike orientations, *Geophysical Prospecting*, *48*, 677-695, 2000.

Godfrey, N., N. Christensen, and D. Okaya, Anisotropy of schists: Contribution of crustal anisotropy to active source seismic experiments and shear wave splitting observations, *Journal of Geophysical Research, 105* (27), 991-1028, 2000.

Johnson, Brann, personal communication, Department of Geology and Geophysics, Texas A&M University, 2004.

Le Masne, D., and G. Vasseur, Electromagnetic field of sources at the surface of a homogeneous conducing halfspace with horizontal anisotropy: application to fissured media, *Geophysical Prospecting, 29*, 803-821, 1981.

McNeill, J.D., Applications of transient electromagnetic techniques, *Geonics Limited Technical Note*, TN-7, 1980.

Melia, P. J. and R. L. Carlson, An experimental test of P-wave anisotropy in stratified media, *Geophysics, 49*, 374-378, 1984.

Moser, S., Proterozoic rocks east and southeast of the Grenville front, Chapter 5: The geology of North America, Precambrian, Conterminous U.S., *The Geological Society of America, C-2*, 1993.

Mutis-Duplat, E., *Geology of the Purdy Hill Quadrangle, Mason County, Texas*, The University of Texas at Austin, Bureau of Economic Geology, 1982.

Nabighian, M. N., Quasi-static transient response of a conducting half-space – An approximate representation, *Geophysics, 44*, 1700-1705, 1979.

Sharma, P. V., *Environmental and Engineering Geophysics*, Cambridge University Press, Cambridge, United Kingdom, 1997.

Song, I., M. Suh, Y. W., and T. Hao, Determination of the elastic modulus set of foliated rocks from ultrasonic velocity measurements, *Engineering Geology, 72*, 293-308, 2004.

Watson, K. A., and R. D. Barker, Differentiating anisotropy and lateral effects using azimuthal resistivity offset Wenner soundings, *Geophysics*, *64*, 739-745, 1999.

Yu, L., and R. N. Edwards, The detection of lateral anisotropy of the ocean floor by electromagnetic methods, *Geophys. J. Int.*, *108*, 433-441, 1992.

APPENDIX A

The paper by al-Garni and Everett (2003) evaluated the electric and magnetic fields in the frequency-domain. Here we will go through the same process. Electromagnetic induction is governed by Faraday's law and Ohm-Ampere's Law with the respective equations

$$\nabla \times \vec{\mathrm{E}} = -\mathrm{i}\omega\vec{\mathrm{B}} \tag{23}$$

$$\nabla \times \vec{\mathrm{B}} = \mu_0 \left(\sigma_{\perp}\mathrm{E}_{\mathrm{x}}, \sigma_{\parallel}\mathrm{E}_{\mathrm{y}}, \sigma_{\parallel}\mathrm{E}_{\mathrm{z}}\right)^{\mathrm{T}} \tag{24}$$

[*al-Garni and Everett*, 2003*]*. Transforming these equations into the horizontal wave number (p, q) domain using Fourier transforms proves convenient [*Yu and Edwards*, 1992]. The Fourier transform pair for 2D space is

$$f\left(p,q\right) = \int_{-\infty}^{\infty}\int_{-\infty}^{\infty} F\left(x,y\right)\exp(+ipx+iqy)dxdy\text{, and} \tag{25}$$

$$F\left(x,y\right) = \int_{-\infty}^{\infty}\int_{-\infty}^{\infty} f\left(p,q\right)\exp(-ipx-iqy)dpdq \tag{26}$$

[*al-Garni and Everett*, 2003]. Faraday's Law (Equation 23) was transformed three times to into the (p, q, ω) domain and then separated into the following components

$$\begin{aligned} \hat{x} &: -iqe_z - \partial_z e_y = -i\omega b_x \\ \hat{y} &: \partial_z e_x + ipe_z = -i\omega b_y \\ \hat{z} &: -ipe_y + iqe_x = -i\omega b_z \end{aligned} \tag{27}$$

[*al-Garni and Everett*, 2003]. Under the same process, Ohm-Ampere's Law (Equation 24) is separated into the following components

$$\begin{aligned} \hat{x} &: -iqb_z - \partial_z b_y = \mu_0\sigma_{\perp}e_x \\ \hat{y} &: \partial_z b_x + ipb_z = \mu_0\sigma_{\parallel}e_y \\ \hat{z} &: -ipb_y + iqb_x = \mu_0\sigma_{\parallel}e_z \end{aligned} \tag{28}$$

[*al-Garni and Everett*, 2003]. These equations are solved and found to obey two separate ordinary differential equations based on the electrical conductivity in the along-strike $\sigma_{\|}$ and across-strike directions $\sigma_{\perp}$

$$\frac{d^2 b_x}{dz^2} - u_{\|}^2 b_x = 0 \tag{29}$$

$$\frac{d^2 e_x}{dz^2} - u_{\perp}^2 e_x = 0 \tag{30}$$

where $u_{\|}^2 \equiv p^2 + q^2 + i\omega\mu_0\sigma_{\|}$ and $u_{\perp}^2 \equiv \sigma_{\perp} p^2 / \sigma_{\|} + q^2 + i\omega\mu_0\sigma_{\perp}$ [*al-Garni and Everett*, 2003; *Yu and Edwards*, 1992] The ordinary differential equations (25 & 26) control the behavior of the electromagnetic field components in the x-direction (across-strike). Applying boundary conditions to these equations allow the field components b_x and e_x to be solved within the uniaxial half-space ($z \to \infty$) and within the upper half-space of air ($z < 0$, $\sigma=0$), respectively

$$\begin{aligned} b_x^1 &= U \exp\left(-u_{\|} z\right) \\ e_x^1 &= V \exp\left(-u_{\perp} z\right) \end{aligned}, \tag{31}$$

$$\begin{aligned} b_x^0 &= C_1 \exp\left(-\lambda z\right) + G \exp\left(+\lambda z\right) \\ e_x^0 &= C_2 \exp\left(-\lambda z\right) + H \exp\left(+\lambda z\right) \end{aligned} \tag{32}$$

where C_1 and C_2 are functions describing the primary field and $\lambda^2 \equiv p^2 + q^2$ is the propagation constant in free-space [*al-Garni and Everett*, 2003]. The al-Garni and Everett (2003) paper gives the following terms describing the primary field

$$C_1(p,q) = \frac{i\pi\mu_0 Iap}{\lambda} \exp(-\lambda h) J_1(\lambda a) \text{ and} \tag{33}$$

$$C_2(p,q) = \frac{-\pi\omega\mu_0 Iaq}{\lambda^2} \exp(-\lambda h) J_1(\lambda a) \tag{34}$$

where J_1 is the order one Bessel function. The remaining unknown coefficients are G, H, U and V. These are found by applying the surface condition (z = 0) to the electromagnetic field components resulting in the following system of equations in matrix form

$$\begin{pmatrix} 1 & 0 & -1 & 0 \\ 0 & 1 & 0 & -1 \\ q/p & 0 & -pq/\tau_{\|} & -\mu_0\sigma_{\|}u_{\perp}/\tau_{\|} \\ i\omega\lambda/p^2 & q/p & i\omega\mu_{\|}/\tau_{\|} & -pq/\tau_{\|} \end{pmatrix} \begin{pmatrix} G \\ H \\ U \\ V \end{pmatrix} = \begin{pmatrix} -C_1 \\ -C_2 \\ -qC_1/p^2 \\ (i\omega\lambda C_1 - pqC_2)/p^2 \end{pmatrix} \tag{35}$$

where $\tau_{\|} = p^2 + i\omega\mu_0\sigma_{\|}$ [*al-Garni and Everett*, 2003]. The coefficients U and V resulting from the analytic solution of these equations are respectively

$$U = ipu_{\perp}\tau_{\|}\Lambda/\omega \tag{36}$$

$$V = -q\tau_{\|}\Lambda \tag{37}$$

where a new parameter $\Lambda$is defined for convenience by

$$\Lambda = \frac{2\pi\mu_0\omega Ia\exp(-\lambda h)J_1(\lambda a)}{p^2u_{\perp}u_{\|} + u_{\perp}\lambda\tau_{\|} + i\omega\mu_0\sigma_{\|}q^2} \tag{38}$$

[*al-Garni and Everett*, 2003]. Inserting U and V into equations 31 and 32, the resulting electric field in the uniaxial medium is expressed by

$$\begin{aligned} e_x^1(p,q) &= \Lambda\left[-q\tau_{\|}\exp(-u_{\perp}z)\right] \\ e_y^1(p,q) &= \Lambda\left[pu_{\perp}u_{\|}\exp(-u_{\|}z) - pq^2\exp(-u_{\perp}z)\right] \end{aligned} \tag{39}$$

[*al-Garni and Everett*, 2003]. In a standard prospecting system, the receiver coil measures the vertical component of the magnetic field, so applying equations 39 to the $\hat{z}$ component of equation 27, the vertical component of the magnetic field in a uniaxial medium is expressed as

$$b_z^1(p,q) = \frac{\Lambda}{\omega}\left[p^2 u_\perp u_\parallel \exp(-u_\parallel z) + i\omega\mu_0 q^2 \exp(-u_\perp z)\right]. \quad (40)$$

Symmetry of p and q allow a 2D Fourier transform to reduce equation 40 to the following

$$B_z^1(x,y,z) = \frac{1}{\pi^2}\int_0^\infty\int_0^\infty b_z^1(p,q)\cos(px)\cos(qy)dpdq \quad (41)$$

[*al-Garni and Everett*, 2003]. For this study, the analysis was taken one more step to convert this equation into the time-domain using Fourier transforms.

Frequency domain electromagnetic surveying systems measure the vertical magnetic field component using a horizontal receiver coil. Under certain conditions, this measurement is shown to be proportional to apparent conductivity σ_{app} with the formula

$$\sigma_{app} = \frac{4}{\mu_0\omega\rho^2}\mathrm{Im}\left[\frac{B_z^T}{B_z^P}\right] \quad (42)$$

where B_z^T is the total magnetic field in the half-space and B_z^P is the primary field produced the transmitter coil [*al-Garni and Everett*, 2003]. Equations of these fields are

$$B_z^T \equiv \mu_0 Ia\int_0^\infty\left[\frac{\lambda^2}{\lambda+u}\right]J_1(\lambda a)J_0(\lambda\rho)d\lambda \quad (43)$$

$$B_z^P \equiv \frac{\mu_0 Ia}{2}\int_0^\infty \lambda J_1(\lambda a)J_0(\lambda\rho)d\lambda \quad (44)$$

where $u^2 \equiv \lambda^2 + i\omega\mu_0\sigma$ [*al-Garni and Everett*, 2003]. The *al-Garni and Everett* [2003] paper further analyzed apparent conductivity as a function of orientation of the transmitter and receiver with respect to the strike of anisotropy in the uniaxial half-space (Figure 2). It was found that the across-strike apparent conductivity $\sigma_\perp$ was greater than the along-strike apparent conductivity $\sigma_{||}$. However, the opposite is true in an electrically

anisotropic medium. The contradiction is due to a paradox of anisotropy in electromagnetic induction where the measurements are controlled by local induced flow. In conclusion, the research by al-Garni and Everett (2003) derived the electromagnetic response of a uniaxial half-space, and found that apparent conductivity varies with transmitter azimuth while submitting to a paradox of anisotropy.

VITA

Jamie Lynne Collins
3906 Figure Four Lake Lane
Richmond, Texas 77469

EDUCATION

Texas A&M University, College Station, TX
M.S. in geophysics, August 2004

Texas A&M University, College Station, TX
B.S. in geophysics, May 2002

EXPERIENCE

Summer 02 GEOPHYSICS INTERN, International Exploration
El Paso Corporation, Houston, Texas

Summer 01 GEOPHYSICS INTERN, Offshore Production
El Paso Corporation, Houston, Texas